EStokTP:

Electronic Structure to Temperature and Pressure Dependent Rate Constants;

A Code for Automatically Predicting the Thermal Kinetics of Reactions

C. Cavallotti[1*], M. Pelucchi[1], Y. Georgievskii[2], S. J. Klippenstein[2*]

[1] Department of Chemistry, Materials and Chemical Engineering "G. Natta", Politecnico di Milano, Milan, Italy

[2] Chemical Sciences and Engineering Division, Argonne National Laboratory, Argonne, IL, USA

*To whom correspondence should be addressed.

E-mail: carlo.cavallotti@polimi.it

Telephone: +39-02-23993176

E-mail: sjk@anl.gov

Telephone: +1-630-252-3596

Abstract

A priori rate predictions for gas phase reactions have undergone a gradual but dramatic transformation, with current predictions often rivaling the accuracy of the best available experimental data. The utility of such kinetic predictions would be greatly magnified if they could more readily be implemented for large numbers of systems. Here we report the development of a new computational environment, namely EStokTP, that reduces the human effort involved in the rate prediction for single channel reactions essentially to the specification of the methodology to be employed. The code can also be used to obtain all the necessary master equation building blocks for more complex reactions. In general, the prediction of rate constants involves two steps, with the first consisting of a set of electronic structure calculations and the second in the application of some form of kinetic solver, such as a transition state theory (TST) based master equation solver. EStokTP provides a fully integrated treatment of both steps through calls to external codes to perform first the electronic structure and then the master equation calculations. It focuses on generating, extracting, and organizing the necessary structural properties from a sequence of calls to electronic structure codes, with robust automatic failure recovery options to limit human intervention. The code implements one or multi-dimensional hindered rotor treatments of internal torsional modes (with automated projection from the Hessian, and with optional vibrationally adiabatic corrections), Eckart and multidimensional tunneling models (such as small curvature theory), and variational treatments (based on intrinsic reaction coordinate following). This focus on a robust implementation of high level TST methods allows the code to be used in high accuracy studies of large sets of reactions, as illustrated here through sample studies of a few hundred reactions. At present the following reaction types are implemented in EStokTP: abstraction, addition, isomerization, and beta-decomposition, Preliminary protocols for treating barrierless reactions and multiple-well and/or multiple-channel potential energy surfaces are also illustrated.

1. Introduction

In recent years, gas phase theoretical chemical kinetics has transformed from an empirical to a predictive science, with achievable accuracies approaching or even exceeding that of experiment. This transformation arises from the dramatic progress in the accuracy of electronic structure calculations, as well as improved procedures for incorporating their results within treatments of chemical dynamics and kinetics. The *ab initio* transition state theory-based master equation (AITSTME) approach,[1] which provides the basis for much of the work in this area, is finding widespread utility as a tool for chemical kinetic modeling.[2-15] This usefulness could be greatly enhanced by reducing the human effort involved in the implementation of such calculations. In particular, a fully automated procedure for accurately predicting rate constants could have a tremendous impact on global chemical modeling of combustion, atmospheric, and astrophysical environments, for example.

A reliable, automated rate prediction procedure would facilitate the use of leadership class computing facilities in predicting rate constants for whole sets of reactions. Furthermore, if that code scales well with machine resources, then it will also significantly increase the size of the reaction system that can be considered. With the imminent transition to exascale computing it should then be possible to automatically create large databases of rate constants. These databases could be used, with machine learning, to devise new and improved rate rules for describing the reactivity of molecules that have not yet been explored either experimentally or theoretically (e.g., for larger molecules in a given class of reactions). This utility would be very useful in developing mechanisms for new fuels, as is being done in the Co-Optima[16] and the Tailor Made Fuels from Biomass (TMFB) projects.[17] An even bolder goal would be to directly determine rate constants for a whole mechanism. Coupling that to an automatic mechanism generator, such as RMG,[18,19] would yield a fully automated procedure for generating fundamentally based mechanisms, without the need to refer to a specific set of rate rules.

Typically, AITSTME calculations are performed in three distinct steps: first the molecular properties of the stationary points on the potential energy surface (PES) are predicted by ab initio (AI) electronic structure calculations. Microcanonical rates for chemical reactions are then determined with transition state theory (TST), with the necessary input data coming from the electronic structure calculations. Finally, phenomenological rate constants are obtained with master equation (ME) solver codes, which take as input microcanonical rate constants and intermolecular energy transfer rates. While transition state theory and master equation calculations are often performed within the same code, electronic structure calculations are almost always performed using separate software. This decoupling of electronic structure and rate constant evaluations leads to considerable human effort wasted on the transfer of data from one set of codes to the other.

The simplest form of TST, with a fixed TS and Rigid Rotor Harmonic Oscillator (RRHO) approximations for the energy levels, takes as input only the geometries, energies, and Hessian of the PES at the stationary points on the PES. However, for high accuracy predictions, one must consider hindered rotor (HR) corrections, variational effects, and tunneling contributions, each of which requires a large number of additional electronic structure calculations. For each separate calculation, inputs must be prepared manually, various failures can happen, and the outputs must be read and checked carefully. Thus, the required human effort can easily became high. In addition, extensive human intervention in managing large sets of data can easily lead to the undesired insertion of random erroneous values that may be difficult to track. Because of this, it is highly desirable that the whole process of estimating rate constants is automated. The many steps involved in the estimation process, together with the presence of occasional methodological failures, makes this a challenging goal to achieve.

The process required for an ideal automatic rate constant estimation code is outlined in the diagram provided in Fig. 1. The first step involves an investigation of the PES to discover the kinetically relevant chemical reaction pathways. This step is required for reactions taking place on a

complicated PES with multiple interconnected wells and products. In contrast, this step is unnecessary if the reaction has a single saddle point that is connected through van der Waals (vdW) wells to the entrance and exit channels for the reactant and products, as for abstraction and addition reactions. Next, geometries and frequencies must be determined for each of the stationary points (minima and saddle points) at the chosen level of theory. This information is sufficient to provide a first order estimate of the rate constant based on conventional TST (i.e., with a fixed TS) coupled with RRHO approximations for the energy levels. However, at this level the predicted rate constants can differ from the true values by more than a factor of 100. Such errors are much greater than the uncertainty of rate constants determined from well-validated rate rules, i.e., those based on scaling of accurate determinations (experimental or theoretical) for chemically similar reactants.

To improve the quality of the rate estimate, a series of additional calculations are necessary. The highest impact on the accuracy of the rate prediction comes from higher-level theoretical estimates of the stationary point energies. Both conformational analyses and a proper treatment of anhamonicities, via, for example, hindered rotor analyses and/or spectroscopic perturbation theory, also contribute significantly to decreasing the uncertainty in the rate predictions. A correct determination of the symmetry of external and internal rotors (if present), and the number of optical isomers is also necessary. Notably, errors in these quantities, which linearly affect the rate constant, are quite common. Furthermore, for one-dimensional hindered rotor treatments it is not always clear what is the best choice for the symmetry correction factor. Finally, intrinsic reaction coordinate (IRC) calculations should in general be included both as a check on the correctness of the presumed pathway, and, more importantly, to allow for the implementation of variational rather than conventional transition state theory.

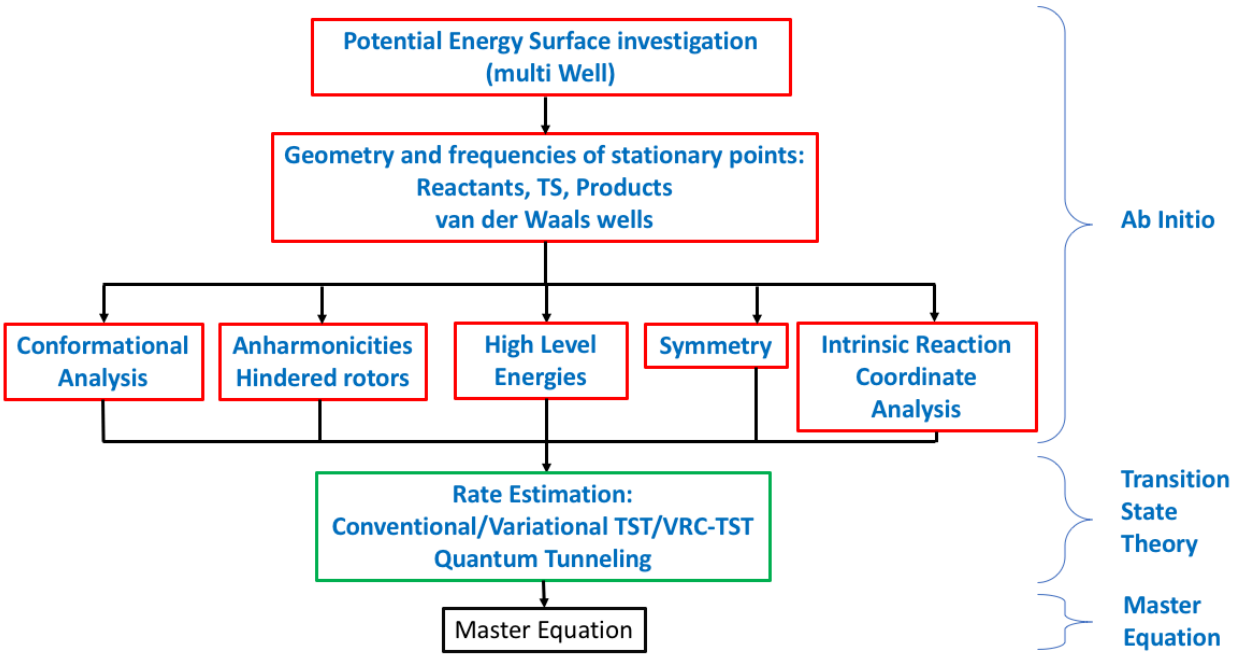

Figure 1. Computational steps required for a protocol that automatically implements an accurate high-level prediction of the rate constant for an arbitrary reaction.

Many codes are available in the scientific literature that can perform either electronic structure or master equation based rate constant calculations. However, the integration of electronic structure and master equation calculations within a single computational environment has rarely been explored. The Polyrate[20] and MS-Tor[21] software from Truhlar and co-workers have long provided access to many of the most advanced implementations of TST available in the literature, with Polyrate providing particularly advanced treatments of tunneling, variational effects, and barrierless reactions while MS-Tor directly addresses the effects of coupled hindered rotors explicitly accounting for the presence of conformers. Polyrate, as well as MSTor, have several hooks and scripts that allow them to run and extract information from electronic structure software. For example, Polyrate and Gaussian are coupled through Gaussrate.[22]

The VaReCoF,[23,24] MESS,[25,26] and NST[27,28] codes from Argonne implement similarly advanced TST frameworks, with VaReCoF providing an advanced treatment of barrierless reactions, while

NST implements non-adiabatic statistical theory, and MESS includes input options for incorporating a wide variety of effects including variational, multidimensional torsions, mode anharmonicity, and tunneling options. Of course, other leading master equation codes, such as MultiWell[29,30] and MESMER [31,32] also implement a variety of TST options. Many of these codes also contain subroutines and scripts that allow them to run and extract information from electronic structure software. However, none of these codes contain robust procedures for locating saddle point structures and evaluating temperature and pressure dependent rate constants directly from a simple specification of the reactants, and there does not appear to have been any attempt to implement them at the scale of automated treatments of large sets of reactions. Here we focus on making connections to the ANL suite of codes, with our initial focus on directly interfacing electronic structure theory to the many options within MESS.

West and coworkers recently presented the first demonstration of the automatic determination of rate constants for a large number of reactions starting from just a reaction list.[33] For this purpose, a dedicated software was developed: Auto TST. It relies on the use of an integrated environment which exploits calls to different codes: Gaussian for electronic structure calculations;[34] CanTherm for the evaluation of partition functions;[35] RMG for mechanism generation;[18] RDKit to generate structural data necessary to determine a guess geometry for the calculation of the transition state.[36] West and coworkers demonstrated a 70% success rate for Auto TST in scanning more than a thousand reactions consisting of various H-abstractions, isomerizations, and additions. With their focus on single-channel pressure-independent rates, Auto TST does not include PES exploration or master equation calculations, which are two key components of the tasks outlined in Fig. 1. Furthermore, rate constants were estimated in only the RRHO approximation using conventional TST, with concomitantly large uncertainties in the computed rate constants (more than a factor of 10).

In the present work, we propose a computational protocol that integrates electronic structure calculations with master equation simulations. The purpose is to create a computational environment that is able to automatically perform the electronic structure calculations needed to apply sophisticated versions of TST and to thereby automatically determine high accuracy rate constants at arbitrary temperatures and pressures through master equation simulations. Importantly, this protocol allows for high-levels of electronic structure evaluations through composite schemes, incorporates high-level transition state theory methodologies with anharmonicity, variational, and tunneling corrections, and it employs state-of-the-art master equation methodologies. Furthermore, the generic input files require a specification of only the reactants and products, the site of reaction, and the theoretical methodologies to be implemented, which should facilitate the implementation of this code over large sets of reactions. This protocol is implemented in software that is freely distributed by the authors: EStokTP.[37]

This work is organized as follows: In section 2 the computational protocol is described. This description begins with an overview and then details of its implementation are given. In section 3 a large number of sample studies are used to demonstrate the success of the effort and to illustrate its utility. First, some guidelines are given on how the protocol can be used to determine rate constants for specific reaction classes and then a statistical analysis of the success of the implemented algorithms is reported.

2. Methods and Algorithms

The EStokTP computational environment is designed to directly couple the electronic structure, TST, and ME evaluations in automatically obtaining *a priori* predictions of temperature and pressure dependent rate constants. The code has been written following two principles. The first is that it must be able to reliably and automatically determine the large number of rate constants describing whole classes of reactions for a target molecule (e.g. H-abstractions). This requirement is

motivated by the desire to take maximum advantage of the upcoming availability of exascale computational resources, as discussed in the introduction. The code is thus robust, with several automatic fallback options implemented so that human intervention can be limited, if not utterly eliminated. The second is that it must be capable of determining highly accurate rate constants, ideally differing by no more than a factor of two from experiments. While this is a reasonable aim for several classes of reactions over wide ranges of temperature and pressure, there are a few situations where such aim is difficult to reach, as discussed at the end of section 2.

In this section, we begin by providing a preliminary description of the EStokTP computational protocol, with further implementational details outlined in the successive subsections and in the manual.[37] The code requires as input the reference molecular structures, the sites and types of transition states to be searched, and the electronic structure and transition state theory methodologies to be employed. Given this set of input files, the code performs the series of calculations listed in Fig. 2.

Initially, the structure of reactants and products are determined at a low level of theory (level 0). Monte Carlo sampling of torsional dihedral angles is used to perform a conformational search designed to locate the absolute minimum energy structure. A guess structure for the transition state is then generated by performing a 1-dimensional grid search as a function of a reaction class dependent interatomic distance. Next, a level 0 transition state is determined from the standard protocols implemented in the electronic structure software supported by EStokTP. At this stage, a conformational search is performed for the TS, with its lowest energy torsional state retained for use in successive calculations. The electronic energy, geometries, and vibrational frequencies of all stationary points (reactants, products, and saddle points) are then determined at a higher level of theory (level 1), using as starting structures those determined with theory level 0. At this point, there is sufficient information to implement an RRHO-based conventional TST analysis at theory level 1.

Various additional calculations allow for improved accuracy rate predictions. First, if desired, structures of the vdW wells that are generally present in the reaction entrance or exit channels can be determined. This vdW analysis can be performed at first level 0 and then level 1, or directly at level 1 from guess structures generated from the TS geometry determined at the corresponding level of theory. The next step in the sequence involves torsional scans for arbitrarily specified sets of dihedral angles. The scans can be performed in 1, 2, or 3 dimensions. Following the torsional scans, the torsional motions of the scanned dihedrals are projected out from the Hessian computed at theory level 1, so that a list of vibrational frequencies reduced by the number of investigated dihedral torsions is generated. If desired, the reaction path is determined through intrinsic reaction coordinate (IRC) calculations, which yields the data necessary to implement variational transition state theory. The symmetry factors, including rotational and optical symmetry, are determined using the symmetry module. Single point energies, such as CCSD(T) energies extended to the complete basis set limit (CBS), are then computed at a high level of theory on level 1 geometries for all of the stationary points. Higher levels energies may also be determined for selected points along the IRC, if desired.

All the data so determined are finally collected in what we call ME blocks. An ME block contains the information needed to construct an ME input section for a given stationary point, and all in a formatting style consistent with the input of the MESS master equation solver. Some examples of ME block structures are reported as supporting information. EStokTP is then able to assemble the ME blocks to create an input file that can be read by the MESS solver and used to determine rate constants for the considered reaction in the desired temperature and pressure ranges.

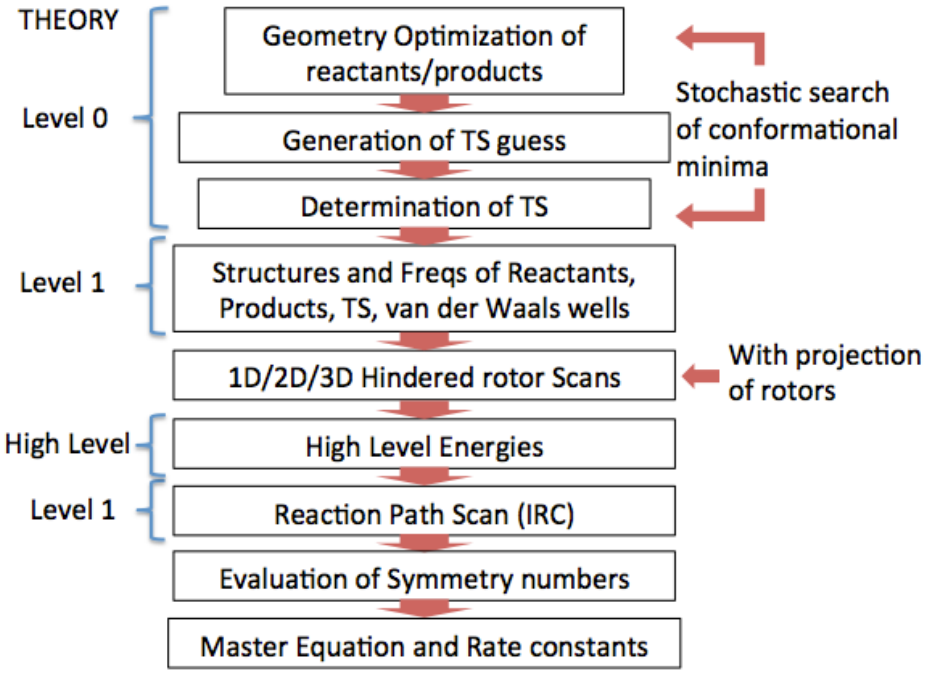

Figure 2. EStokTP program structure.

As anticipated, EStokTP relies on calls to external codes to perform the electronic structure and master equation calculations. At present Gaussian and Molpro are supported for electronic structure calculations and MESS for master equation simulations. Tunneling in EStokTP can be accounted for using both the Eckart model[38] and the multidimensional small curvature tunneling (SCT) model of Truhlar and coworkers.[39]

2.1 Strategy for Level 0 geometry searches

There are a variety of strategies that could be used in employing electronic structure theory to determine the minimum energy structures corresponding to the stationary points on PESs. One of the most important aspects of such strategies is the choice of coordinates to be used in performing the optimizations. Common choices are internal, redundant, or Cartesian coordinates. One key focus of EStokTP involves the automated determination of the conformational minima for each species, which we accomplish via Monte Carlo sampling. This focus leads us to use internal coordinates in the geometry optimizations for the reactants, products, and saddle points.

The user is thus required to write a Z-matrix for each reactant and product involved in the reaction. Dihedral angles must be specified so that they properly describe the mutual rotation of two molecular fragments with respect to an intramolecular bond that may lead to conformational isomers. An important requirement is that the internal molecular structure of each fragment should remain unchanged upon a modification of the dihedral angle, which should thus affect only the relative orientation in space of the two moieties. From this Z-matrix, the user must prepare a list of dihedral angles defining the conformational space of the considered molecule.

A companion code, x2z,[40] provides a convenient procedure for converting from Cartesian coordinates to the requisite Z-matrix coordinates. It also directly provides the list of conformationally relevant dihedral angles. In a related project, the x2z code has been used to facilitate automated implementation of EStokTP in the determination of the thermochemical properties for hundreds of species.[41]

From these Z-matrix inputs, EStokTP generates a user specified number of starting structures with randomly chosen dihedral angles. Then, for each generated guess structure a minimum energy geometry search is performed according to the user specified electronic structure method and software. We typically set the number of starting structures to the minimum of ($5+3^{nrotor}$) and 100 configurations, where nrotor is the number of non-methyl rotors.[41] This expression yields a number that grows in proportion to the expected increase in the number of minima with increasing torsional degrees of freedom. The constraint to 100 or fewer configurations maintains the calculation at a manageable level, with our experience being that after this many sampling points either the global minima or some close approximation to it have already been discovered (at least for molecules with not too many torsional degrees of freedom). This Monte Carlo search is performed at theory level 0. The minimum energy structure so determined is then used for successive calculations.

The geometry search procedure for saddle points differs from that for reactants and products. First, the transition state (TS) Z-matrix is not specified by the user, but rather is constructed automatically

by the code on the basis of the Z-matrices of the reactant(s) (one or two depending on the reaction type). For abstraction and addition reactions, the TS Z-matrix is obtained by merging the structures of the two reactants, whose relative separation and orientation is then defined by a number of degrees of freedom that depends on the involved number of atoms (three for a reaction with an atom, five for a linear species, and six for the others). For the most general case of two nonlinear polyatomic reactants, there are six transitional degrees of freedom consisting of one bond length (R_{TS}), two bond angles, and three dihedral angles. Initial guess values for the five angles must be specified by the user, although the success or failure of the code is not really sensitive to these values. Meanwhile, the bond length is used as a frozen coordinate to perform a grid scan within a given length interval and for a given number of steps. The user must also specify three atomic centers that determine the connectivity between the two molecules. Additional information on the set up of the Z-matrix is provided in the EStokTP manual.

With this specification of coordinates, the TS search then begins with a grid-based sequence of geometry optimizations for constrained interfragment bond lengths. Notably, while many of the individual grid-based optimizations may fail, all that is required for the successful implementation of the algorithm is that one is successful. The remaining failed optimizations are simply presumed to lead to low energy states that can be ignored. Next, the geometry of the maximum energy point determined in the grid scan is used as a guess for the TS search, which is also performed in internal coordinates. This search uses the TS search algorithm implemented in the chosen electronic structure code.

For abstraction reactions, a dummy atom that is bound to the abstracted atom is added to the TS Z-matrix to avoid problems related to linear bond angles. For example, the structure of the Z-matrix constructed by the code to study the H-abstraction from methyl acetate by OH is shown in Fig. 3.

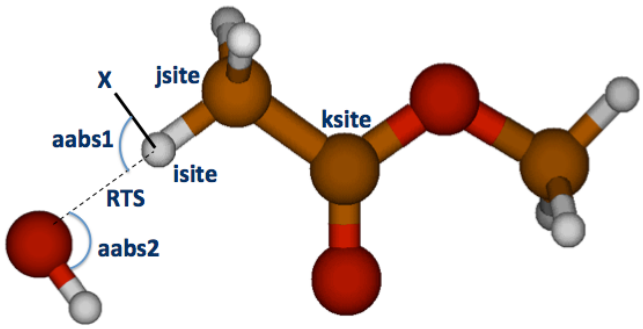

Figure 3. Transition state geometry constructed automatically for H-abstraction in the OH + methylacetate reaction.[42] The atomic centers used to the define the connectivity of the two reacting groups (isite, jsite, and ksite), the scanned distance (R_{TS}), and the two transitional mode angles (aabs1 and aabs2) are explicitly shown, as well as the dummy atom (X).

For abstraction reactions, both forward and backward reactions are abstractions, and one might consider the reaction from either direction. If there is a large difference in the strengths of the bonds that are formed/broken in the reactive process, then EStokTP may only produce good transition state guesses if the coordinate R_{TS} corresponds to the stronger of the two bonds. In other words, when the enthalpy of reaction is large in magnitude, it is generally best to investigate the reaction in the direction that proceeds exothermically, as is the case for the example shown in Fig. 3. To facilitate this requirement, it is possible for EStokTP to automatically change the scanned grid coordinate, thus constructing a different Z-matrix, by simply activating a switch condition. This feature proves useful when scanning families of abstraction reactions made by a single reactant and a series of abstracting radicals (see Section 3.2).

Since beta-scission and isomerization reactions are both unimolecular processes, the Z-matrix for the TS is instead constructed from that for the single reactant. For these cases, the user must simply specify the two atoms involved in the bond-breaking (beta-scission) or formation (isomerization) process. The isomerization and beta-scission algorithms then decrease/increase the distance between the two selected atoms progressively; first with a coarse step from that of the starting

structure to an intermediate distance, and then to a final distance with a finer step. The maximum energy structure from this scan is then used as the TS guess for a standard electronic structure code-based TS optimization.

When studying an isomerization reaction, the chosen starting structure is taken to correspond to the conformer from the Monte Carlo search that exhibits the minimum value for the length of the forming bond, rather than the minimum energy conformer of the reactant. Furthermore, the Z-matrix line that contains the reacting atom is substituted with a line where the forming bond appears explicitly.

For each reaction type, once a TS structure has been located, the same stochastic algorithm used to investigate the conformational space of the wells is again used for the TS. The list of scanned dihedrals must be supplied by the user. The minimum energy structure located in the stochastic scan is then retained for the successive steps. Extensive testing of the combination of the stochastic search and torsional scan algorithms has shown that sometimes the optimizations may converge to saddle point structures connecting undesired wells. In order to determine when this happens, and to thereby remove the structures from the list of TS conformational structures, the structures determined in the stochastic search are compared to those determined after the grid scan. If the difference between R_{TS} (i.e., the scanned bond length) in the two structures is larger than some threshold tolerance, the new structure is discarded.

A different approach is used to find the structures of the reactant and product vdW wells. While the user has the option of specifying the Z-matrix of the wells, the preferred approach is to use the TS Z-matrix as a guess for the vdW search, displacing the bond length of the distance used for the grid scan in the reactant or product directions. This approach is preferred both because it is more stable, and because it produces a structure that is more directly relevant to predicting tunneling rates. This procedure can be performed with the usual sequence starting at theory level 0 and proceeding to level 1, or by starting directly at theory level 1. Extensive testing has shown that the use of either

redundant or Cartesian, rather than internal coordinates leads to a much better success rate in these searches for the vdW minima. Thus, the default option for the determination of the structures of the vdW wells is to use redundant coordinates. A set of additional bond distances suitable to describe the relative orientation of the two reacting molecules is selected automatically and added to the coordinate set used in the optimization.

2.2 Level 1 determination of geometries and vibrational frequencies

Improved structures for each of the stationary points are determined using level 0 structures as guesses. These "level 1" structures are used as reference structures for the rate constant predictions, e.g., to determine rovibrational partition functions, high level energies, and symmetry numbers. Vibrational frequencies are determined at the same level of theory. Hessians in Cartesian coordinates are also computed and saved for subsequent hindered rotor calculations, if needed. The coordinates employed in these level 1 optimizations are the same as those used in the level 0 calculations, i.e., internal coordinates are used to determine the structures of the reactants, products, and saddle points, while redundant coordinates are used for the vdW wells.

Typically, these level 1 calculations differ from their level 0 counterparts in the choice of the basis set. However, an improvement in the quality of the theory is also possible. For example, a level 0 calculation might implement the range separated ωB97XD density functional theory[43] with a modest 6-31G* basis,[44] while the level 1 analysis might implement a double hybrid method such as B2PLYP-D3[45,46] with a cc-pVTZ basis.[47]

Vibrational anharmonicity can have an important impact on rate constant estimation, both at low and high temperatures.[48,49] To address this issue, at present we are working on implementing vibrational second order perturbation theory (VPT2) in EStokTP.[50] An alternative approach is to scale frequencies using empirical factors fitted over experimental databases, as suggested by Truhlar and co-workers.[51] This is the approach presently implemented in EStokTP.

2.3 Torsional motions

Following level 1 calculations, EStokTP is able to perform one, two, and three dimensional torsional scans for a given list of dihedrals. The resulting potential energy as a function of the dihedral angle(s) is then used as input in the rate prediction code. The calculations are organized as follows. First, 1D torsional scans are performed for all scanned dihedrals, even if a 2D or 3D HR scan is requested as they make use of this information in determining the connectivity of the mutually rotating moieties. Following these 1D rotational scans, the torsional motions for each rotor are projected out from the Hessian, which was previously obtained in the level 1 calculations. This projection yields an updated list of frequencies from which the torsional vibrations have been automatically removed. After projection, the hindered rotor PES and the projected frequency list are saved for successive calculations.

The procedure for this projection has been adopted from that proposed by Green and co-workers,[52] with our implementation strictly mimicking that reported in RMG.[18,19] Nevertheless, a dedicated code has been written *ex novo* for this purpose, as EStokTP has been designed to be a standalone code. There is, however, a slight difference between the EStokTP and the RMG implementation of this theory. In RMG the molecule is divided into two portions, one mutually rotating with respect to the other along the connecting bond. In EStokTP, the connectivity of the two molecular moieties is first examined by inspecting each bond length. If a bond is longer than a given threshold, then the portion of the molecule to which it is connected is not included in the molecular block for projection.

A situation where this revision is significant is illustrated in Fig. 4. For this transition state describing the H-abstraction from dimethylether by CH_3, the RMG approach, which is successful for essentially all stable species and most TS analyses, projects out the wrong frequency (100 cm^{-1} computed at the M06-2X/aug-cc-pVTZ level[53]) rather than the correct 236 cm^{-1} frequency. This has an impact of about a factor of 2 on the rate constant at temperatures relevant to combustion (1000-

1500 K). However, it should be noted that the approach implemented in EStokTP relies on the use of a database of critical bond lengths that has been developed on the basis of extensive, though not exhaustive benchmarks, performed mostly on molecules containing C, H, or O atoms. As both RMG and EStokTP approaches are available in the EStokTP suite, it is suggested to check carefully situations where they give different predictions.

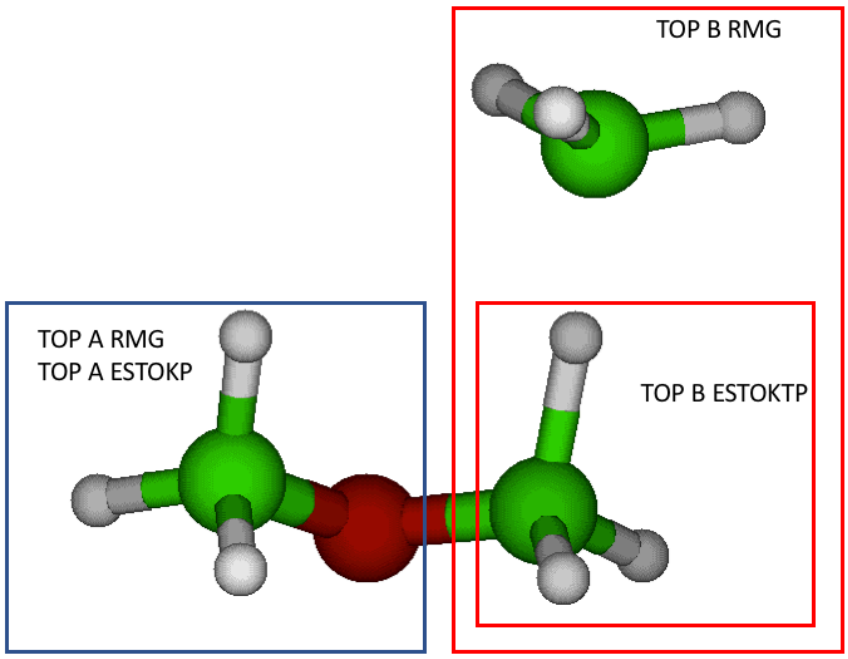

Figure 4. Schematic diagram of the rotating tops identified by RMG and EStokTP for the transition state corresponding to H-abstraction by CH_3 from dimethylether.

Notably, additional features of EStokTP allow us to take advantage of the advanced capabilities of the multi-dimensional hinder rotor treatment implemented in the MESS suite,[25] which is the default master equation solver for EStokTP. In particular, EStokTP can compute the potential and vibrational frequencies at each point of the dihedral scan, from which torsional motions can be projected as described above. These data are then exploited by MESS through a convolution of the vibrationally adiabatic densities of states for the non-torsional internal degrees of freedom with the external rotation density of states and partial local torsional states densities. The result is then integrated over the torsional angles with the torsion-dependent energy shift and mass factor.

To account for quantum effects associated with the torsional degrees of freedom, the Schrodinger equation for the coupled torsional motions is formulated for zero-angular momentum and solved for low energy levels providing the quantum correction to the classical density of states. At higher energies, the quantum density smoothly approaches the classical one, and the quantum corrections are not needed. The dependence of external rotation parameters on the internal quantum state is approximately accounted for by averaging the external rotation mass factor over the internal quantum state. This approach ignores the dynamical coupling between internal and external rotation. To facilitate the computation of the eigenvalues, a Fourier representation of the potential is obtained from a multidimensional product grid of potential values, as described earlier. A similar Fourier representation is employed for the generalized mass matrix and the Hamiltonian is formulated in a Fourier harmonics basis.

2.5 Symmetry

As mentioned in the introduction, a correct determination of the symmetry factors for each of the stationary points considered in the calculation is essential to the accurate prediction of rate constants and thermodynamic parameters. The relevance of using proper symmetry numbers in the determination of rate constants was discussed thoroughly by Pollak and Pechukas[54] and more recently by Fernández-Ramos et al.[55] In EStokTP the external rotational and optical symmetry numbers are first determined through the symmetry code that is part of the MESS suite. This code works by first permuting all groups of identical atoms and determining whether or not the distance matrix for the permuted species are equivalent to the original distance matrix to within some tolerance. If they are, then an additional check for reflection symmetry of the permutation is performed by taking the scalar triple product for 3 nonplanar atoms in the species. If this product changes sign then this permutation does not contribute to the rotational symmetry number. Furthermore, if this cross product changes sign for any one of the permutations, then the molecule does not have an enantiomer. Otherwise, it does.

The hindered rotor PES is then scanned to check for the presence of degenerate isomers along the rotational scan. For this purpose, all minimum energy structures along the dihedral scans are re-optimized at the chosen level of theory. If the computed energy differs by less than a given energy threshold from the absolute minimum energy, than the new minimum is considered as a degenerate isomer. Finally, a global symmetry factor is computed as the product of the external rotational symmetry number and the number of torsional isomers found divided by the external optical isomer number. Note that this algorithm has not yet been extended to treat degeneracies in multidimensional hindered rotors, in which case direct user intervention is needed to set the proper symmetry factor.

2.6 High level energy determinations

High level energies are computed at the level 1 geometries for each of the stationary points considered in the reaction network. Typically, calculations at the CCSD(T) or CCSD(T)-F12 level, with basis sets of triple-ζ or better quality, are particularly effective in obtaining high accuracy kinetic predictions. As supported by the electronic structure codes, these calculations may include composite combinations to approximate, for example, the complete basis set limit. With increased molecular size for the investigated system, such CCSD(T) calculations rapidly become the most expensive part of the calculations, in terms of CPU, storage, and memory usage.

2.7 Intrinsic reaction coordinate scans

For the next step, optional intrinsic reaction coordinate (IRC) scans can be performed to study the molecular evolution along the reaction path. Such calculations help to confirm that the specified TS connects the desired reactants and products. Perhaps more importantly, the structures, energies, and vibrational frequencies determined along the reaction path can be used to obtain variational corrections to the conventional TST rate predictions. For this purpose, it is best to perform the IRC scans by computing the Hessian at each point along the reaction path. Torsional motions are then projected from the Hessian and vibrational frequencies are computed for each point along the

reaction path. It is also possible to choose whether to update the hindered rotor PESs along the IRC path, or to simply keep the HR PES computed at the saddle point. The latter is often a reasonable choice since the density of states of the hindered rotor partition function tends to have only a mild dependence on the height of the HR PES. In order to be consistent with the set of vibrational frequencies computed at theory level 1, IRC calculations must be performed at the same theory level 1.

The vibrational frequencies calculated along the MEP depend on the chosen coordinate system, with all coordinate systems converging to the same values only at stationary points, where the energy gradient is zero. It has been shown for many reactions that Cartesian vibrational frequencies computed along the MEP can give unphysical values, for example becoming imaginary even in proximity of the saddle point.[56] This can have an important impact on the evaluation of rate constants. To address this important issue the possibility to compute vibrational frequencies in curvilinear coordinates has been implemented in EStokTP as suggested by Truhlar and co-workers.[57] The main difference is that the Wilson B matrix and the C matrix, representing the first and second derivatives of the internal coordinates with respect to Cartesian displacements, are computed using finite central differences. The currently implemented internal coordinates are nonredundant coordinate systems consisting of bonds, angles, and torsions. As EStokTP uses Z-matrices to perform optimizations and TS searches, the Z-matrix set of coordinates can be directly used to determine frequencies in curvilinear coordinates. Alternative coordinate sets can be specified directly by editing the Z-matrix. To test the correctness of our implementation, vibrational frequencies were computed using curvilinear coordinates with both EStokTP and Polyrate for reactions that are sensitive to a change of coordinates, such as the H_2 + OH abstraction and C_2H_4 + H addition reactions. The agreement was quite good, with vibrational frequencies differing by at most about 10 cm^{-1}, but in general being more or less superimposed.

The energy along the reaction path must also be consistent with the high-level energies for the reactants, products, and TS. For this reason, the energy profile is by default shifted to match the energy barrier computed at the saddle point at the chosen level of theory. In addition, high-level energy evaluations may be performed for a specified number of points along the reaction path. If this number is smaller than the total number of IRC steps, then the energy of the missing points is re-scaled in accord with the available ones.

2.8 Tunneling

Quantum tunneling contributions to rate constants can be computed using two different models. The first is the simple asymmetric Eckart model. For this purpose, energy barriers are determined relative to either the reactants and products, or the vdW wells if they are considered. These energy barriers together with the imaginary frequency value provide the necessary input for the MESS solver to implement Eckart tunneling corrections.

Alternatively, Small Curvature Tunneling (SCT)[39] corrections can be implemented using reaction path Hamiltonian frequencies[58] or curvilinear coordinates.[57] Both temperature dependent tunneling contributions and imaginary action integrals can be determined. The latter can be taken as input by the MESS solver. It should be pointed out that SCT theory requires IRC calculations on a sufficiently extended path. Typically, on the order of 100 points in both the reactant and product directions using a step of 0.02 bohr are necessary to obtain converged results.

2.9 Rate constant estimation

The final step of an EStokTP job involves the prediction of the temperature and pressure dependent rate constants for the specified reaction. This step is only performed after the completion of all the preliminary steps outlined in Fig. 2. Within EStokTP we have implemented four different computational protocols for automatically predicting the rate constant for the four different reaction types: abstraction, addition, beta-scission, and isomerization reactions. A fifth protocol is also being

developed for barrierless reactions, as discussed below in section 2.9.5. With these protocols, given a proper set of input parameters, the rate constant prediction procedure then proceeds without human intervention by performing in succession all the steps outlined in Fig. 2.

2.9.1 Abstraction

In general, IRC following forward and backward from an abstraction TS leads to the formation of two vdW wells rather than directly to bimolecular reactants and products. These vdW wells are submerged below the energy of the corresponding bimolecular species (cf. the schematic PES sketched in Fig. 5). As a result, there are really three distinct transition states for any abstraction reaction. One describes the formation of the entrance channel vdW well, the second describes the actual abstraction process, while the third describes the decay of the exit channel vdW well. The first and the third transition states generally correspond to barrierless processes and do not have a saddle point associated with them. Phase space theory provides an effective procedure for qualitatively estimating the reactive flux for such barrierless TSs.

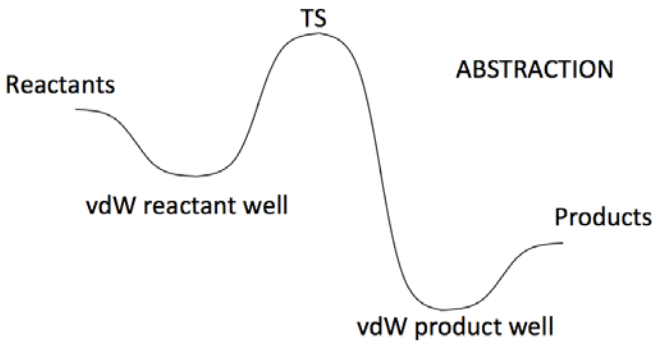

Figure 5. PES used to calculate thermal rate constants for abstraction reactions using a three transition state (3TS) model.

Three different models have been implemented within EStokTP to predict rate constants for such abstraction reactions. They differ in whether or not van der Waals wells are considered for both the reactant and product sides (3TS calculation), for only the reactant side (2TS calculation), or not at all (1TS calculations). The schematic diagram in Fig. 5 illustrates the PES for the 3TS model, with

the 2TS and 1TS abstraction PESs differing only in the absence of the vdW product well and in the absence of both vdW wells, respectively. Most theoretical studies in the literature consider only the single abstraction TS of our 1TS approach. However, we find that it is often useful to include at least qualitatively the effect of the two other TSs.

In the 3TS model, the rate constant for the full abstraction process is computed by solving the master equation for the three channels: entrance, exit, and abstraction. The microcanonical rates for the long-range part of the entrance and exit channels are computed using phase space theory with a $1/R^6$ potential.[59,60] Alternative potentials of the form $1/R^n$ may also be employed. Such potentials provide an adequate representation of the long-range collision rate. The automated implementation of better treatments such as variable reaction coordinate TST is much more challenging and so is left for future work. Phase space theory calculations are set up and performed automatically by the MESS solver. If VRC-TST calculations have been performed offline, then it is straightforward to edit the ME solver input produced by EStokTP to implement the results of those calculations in the evaluation of the overall rate constant. The microcanonical rates for the abstraction itself are determined using the transition state theory procedures outlined above.

Usually, the rates of the entrance and exit channels greatly exceed those of the abstraction channel, with passage through the abstraction transition state being the rate controlling step. However, at sufficiently low temperatures the vdW wells may live long enough to be collisionally stabilized. In this case, they appear as a product channel in the master equation results, carrying important implications for low-temperature gas phase chemistry. Furthermore, the depth of the vdW wells may have a significant impact on the quantum tunneling contribution to the rate constant, especially at low temperatures and when the reaction barrier height is small with respect to reactants. Thus, it is advisable to compute the energy and structure of the vdW wells at the same level of theory as that of the reactants and products.

Unless the rate of stabilization of the vdW well is of specific interest, it is generally not necessary to perform a hindered rotor study of the vdW wells. If performed, hindered rotor studies of the vdW wells should be carefully checked as they may easily lead to other vdW wells, which may not be those connected to the reaction transition state. In reality, quantitative estimates of the state densities for the vdW wells would be better accomplished through direct phase space sampling. Furthermore, in most instances, there are really multiple vdW wells for both reactants and products and one should design formalisms that include and treat the transformations between each of them. For now, we have left such improvements for later work.

Using a master equation solver to determine rate constants for abstraction reactions is somewhat unusual as these reactions are generally pressure independent and thus, in principle, do not require a master equation treatment. There are however a number of advantages in studying the kinetics of such reactions with a ME treatment. The first is that the 3TS ME treatment is one of the possible approaches to properly limit the contributions to the reactive flux from energy states below the asymptotic energies of the fragment. In particular at low pressure, only states above the reactants and product asymptote should contribute to the reactive flux, while at pressures where stabilization occurs, which can be reached at low temperatures especially for vdW species with intermolecular hydrogen-bonds, subthreshold states may contribute to the kinetics. Such proper physical limits on the reactive flux contributions are particularly important when computing quantum tunneling corrections to the rate coefficients. A second reason is that the phase space theory estimates for the entrance and exit channels can pose significant constraints on the overall reactive flux, particularly at higher temperatures and for reactions where the abstraction saddle points are submerged below the reactants or products. A third reason is that this approach allows for a treatment of stabilization in the van der Waals well, such as may occur at the low temperatures of relevance to astrochemistry. Finally, this procedure also provides a basis for properly analyzing the branching between different abstraction channels through planned generalizations to include isomerizations between multiple vdW wells.

2.9.2 Addition

An entrance channel vdW well almost always plays a similar role for addition reactions as it does in abstraction reactions. Thus, within EStokTP we have implemented two alternative PES schemes (2TS and 1TS) for the evaluation of the temperature and pressure dependence of addition rate constants. A schematic diagram of the 2TS PES is provided in Fig. 6. For the corresponding 1TS scheme, the vdW reactant well is absent.

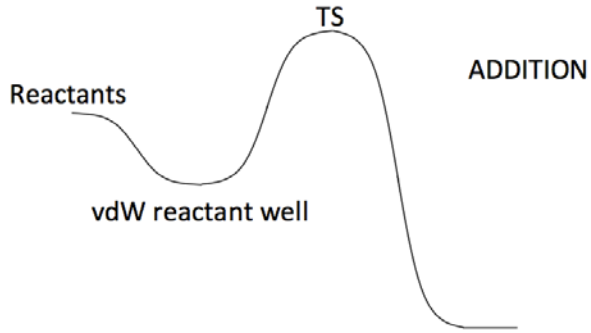

Figure 6. PES used to calculate addition reaction rate constants using a two transition state (2TS) model.

Again, as described above for abstraction reactions, for the 2TS model the addition rate constant is computed by solving a master equation consisting of two channels: the entrance and the chemical addition. The microcanonical rates for the entrance channel are computed using phase space theory, while those for the chemical addition channel are determined using the transition state theory methods described earlier. In contrast with abstraction reactions, the solution of the master equation is generally necessary for addition reactions due to the possibility for redissociation of the product (i.e., the chemically transformed addition complex). This redissociation of the chemical complex leads to a pressure dependence of the rate constant that is effectively treated with the master equation.

For now, the input file for the master equation calculations also requires parameters describing the collisional energy transfer for the reacting system under investigation (i.e., the parameter ΔE_{down} describing the average downwards energy transferred and the Lennard Jones parameters for the reactants and products). Independent work by Jasper and coworkers[61,62] may allow us to automatically generate these parameters.

2.9.3 Beta-scission

Since beta-scissions are the reverse of additions, their rate constants may be determined through detailed balance from the addition rate constant. Alternatively, EStokTP also includes an algorithm that focusses directly on the beta-scission reaction, and it is sometimes preferable to employ this algorithm. For example, the beta-scission algorithm tends to be more effective when the barrier to decomposition is quite low, with a corresponding very modest increase in the bond length for the decomposing bond from its value in the complex. The rate of the beta-decomposition reaction is determined by solving the master equation with the MESS code, so that pressure dependence is properly accounted for. As for addition reactions, proper energy transfer parameters must be assigned prior to performing the master equation calculation. At present, no vdW well model is implemented for this type of calculation.

2.9.4 Isomerization

Isomerization reactions are treated as pressure dependent unimolecular processes that involve one reactant and one product. The isomerization algorithm can also be used to study elimination reactions, although, due to the simplicity of the TS locating procedure, the failure rate for these processes can be significant. Alternatively, it is possible for EStokTP to import transition states located using other codes, such as the GSM code of Zimmermann[63] or the STN approach of Peng and Schlegel.[64] To do so simply requires that a TS geometry is provided in internal coordinates with a Z-matrix that has properly assigned dihedral angles (see Section 2.1). Again, the x2z code, which is available as a companion to this work, facilitates the preparation of this data.

2.9.5 Barrierless reactions

At present EStokTP does not contain a fully automatic algorithm for predicting rate constants for barrierless reactions. However, there are two approaches that can be used to set up reasonable variational TST calculations for such reactions. Both approaches rely on first performing calculations that freeze a selected Z-matrix bond length at a given value. Level 0 and level 1 calculations, Monte Carlo conformational scans, and hindered rotor scans can then be performed at the frozen distance. A good guess for the initial frozen geometry can be generated using the grid scan that is usually performed as a prelude to the TS search.

Two alternative procedures could be used to proceed on to predicting the rate constant. First, the points along an IRC calculation starting from the frozen geometry can be used to build a variational input for MESS. Alternatively, the frozen reaction coordinate calculation can be repeated for different bond lengths (as many as desired) through separate EStokTP calculations. The data thus generated can be collected through a script and again used to set up a variational input file for MESS. In both instances, the MESS master equation solver can then be used to obtain pressure dependent rate predictions. The latter approach allows for the implementation within electronic structure codes that do not perform IRC analyses, thereby facilitating multireference calculations for example. It also provides an alternative for cases where the underlying IRC analyses fail due to the low gradients at long-range.

An approach that is consistent with the current implementation of EStokTP is to use the CASPT2 theory within Molpro. A reasonable active space can be selected for some initially chosen bond length. The same set of calculations can then be repeated for a range of bond lengths scanning the range of variational TSs, with careful checking for consistency in the active space. Notably, EStokTP allows for a rescaling of such CASPT2 energy changes in the construction of the final variational PES. For example, the ratio of a CCSD(T)/CBS based evaluation of the bond energy to the CASPT2 based one could be used to scale the CASPT2 IRC energies. Over the longer term,

directly coupling to VaReCoF based VRC-TST calculations should provide a route to increased accuracy. It should however be mentioned that at present, if such VRC-TST calculations have already been performed offline (e.g., with the VaReCoF code), then it is straightforward to edit the ME solver input produced by EStokTP to implement those results in the ME analysis.

2.10 Accuracy of the AITSTME approach

As stated at the beginning of this section, one of the goals of EStokTP is to provide a theoretical framework that allows for high accuracy rate predictions. For most reactions, we aim to achieve an accuracy of about a factor of 2 or better with respect to nominal values. At high temperatures this appears readily achievable, while near room temperature further progress in barrier height and tunneling estimation may sometimes be needed. Occasionally, TST is inaccurate because the basic assumptions of TST (ergodicity, non-recrossing, semiclassical expressions) are of limited accuracy. In particular, in some cases the energy is not randomized among all the molecular degrees of freedoms, which can lead, among other things, to a situation where some of the potential wells are not explored (e.g., in the exit channel). When this happens, the reaction is said to be non-RRKM and AITSTME predictions of rates and branching ratios can become significantly inaccurate.[65,66] This is for example the case for the S_N2 reaction between OH- and CH_3F.[66] Though it is difficult to predict a priori whether a reaction may exhibit non-RRKM behavior, there are only a few examples of non-RRKM thermal reactions reported in the literature. When AITSTME fails, the most proper approach is to study the reaction dynamics using trajectory simulations, for example through direct dynamic simulations using density functional theory (DFT) energies and gradients.[67] Fortunately, for thermal reactions, such failures appear to be quite limited, as demonstrated by the success of AITST calculations in reproducing large bodies of rate measurements.

Also, even when the energy is properly randomized among the internal and external degrees of freedom, there are still several situations where the uncertainty in the rate constants predicted by AITSTME as implemented in EStokTP becomes intrinsically larger. For example, when the rate

constants are pressure dependent, as with addition and recombination reactions, uncertainty in the collisional energy transfer parameters leads to modestly increased uncertainties in the rate predictions. Furthermore, the proper description of the collisional excitation/equilibration process requires a description of not just the collision-induced transitions in energy but also of the transitions in the total angular momentum (J).[68] To properly describe the effect of those transitions requires a 2D master equation (in E and J), rather than the 1D ME currently used in EStokTP.

The level of uncertainty of the rate constant calculations is also expected to increase when reacting systems having several coupled internal rotors are considered, especially when some structures involve hydrogen bonding interactions. While this can be addressed in EStokTP using the implemented multidimensional vibrationally adiabatic hindered rotor model, a thorough validation of this approach with respect to experiments or to alternative theoretical approaches, such as those implemented in MS-Tor,[21] is needed to properly determine its accuracy.

Two other situations where the accuracy of rate constants determined using the approaches implemented in EStokTP is expected to decrease are very low and very high temperatures. At very low temperatures the uncertainty is related to that of barrier heights and to the adopted tunneling model, while at high temperatures anharmonic effects (and multiple electronic states) can impact significantly the estimation of the rovibrational density of states, and thus the rate constant estimation.

One of the utilities of the EStokTP code that we foresee is its facilitation of careful benchmarking of the success and failures of various possible implementations of the AITSTME approach through widespread application to large numbers of reactions. Such studies will help us better understand the extent of the errors introduced by these various concerns.

3. Results and Discussion

In the following, sample applications of EStokTP to the study of abstraction, addition, isomerization, beta-scission, barrierless, and a complex multichannel reaction are reviewed. This survey begins with a review of EStokTP calculations for the simpler case of the thermochemical properties of molecular species, i.e., reactants or products or wells. This application provides a direct indication of the success and utility of many subcomponents of the code. For both the abstraction and addition cases, EStokTP was applied to on the order of 100 distinct reactions. This extensive testing allows for statistical analyses of the code success rate. For these reactions, some limited comparisons of EStokTP predictions with literature results are also provided to illustrate the predictive success of sophisticated a priori TST. More substantial comparisons will be provided in future system specific applications studies. For the remaining cases, we restrict our discussion to more qualitative commentary on the expected utility of the code.

3.1 Wells

The determination of the structural and rovibrational properties for a given molecular species, which is a key step in each of the rate analyses, is also of utility in determining thermochemical properties. Such molecular species studies represent the simplest of the EStokTP runs. In the most complicated situation, the molecule has several coupled internal rotors. In this case, the set of calculations that should be performed are schematized in Fig. 7.

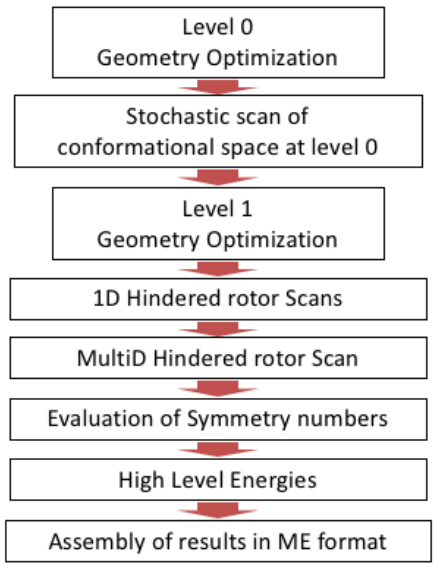

Figure 7. Sequence of EStokTP modules that can be called in order to determine the molecular properties of a given species.

The sequence of steps reported in Fig. 7 yields the minimum energy geometry of a molecule and its vibrational frequencies determined at theory level 1, as long as a sufficient number of random geometries were included in the stochastic conformational search. Then, 1D hindered rotor potentials are computed for motions relative to that minimum energy structure and the corresponding frequencies are projected from the Hessian matrix. After that, a multidimensional hindered rotor (up to 3D) PES may be mapped out and projected frequencies may be computed at each point in the scan. Symmetry numbers can then be determined using the combined MESS (external symmetries) and EStokTP (internal HRs symmetries) algorithms. Finally, the energy can be computed at a high level of theory and all the results collected in a ME block format (see above).

It should be noted that all the calculation steps reported in Fig. 7 can be run either as a continuous sequence from beginning to end, without any need of human intervention, or one at a time. This type of flexibility can be exploited by external codes that use just some of the functionalities of EStokTP to determine the parameters of interest. For example, in related work,[41] a set of scripts were developed (primarily, QTC[69] and TorsScan[70]) that generate high level thermochemical data for

large sets of species (e.g., 100-1000), as in typical combustion kinetic mechanisms. Within this predictive automated combustion thermochemistry (PACT) process the TorsScan script generates the EStokTP inputs and then calls the EStokTP code to perform the stochastic search for the minimum energy conformer of a given species, to determine the one- and multidimensional hindered rotor potentials, and to evaluate the projected vibrational frequencies. The initial application of this approach generated thermochemical data for 163 species in a low-temperature butane oxidation mechanism, with a 98% success rate, although a few symmetry numbers and electronic degeneracies did need to be corrected.[41] Continuing work in progress is finding similar success rates for other equivalently large combustion species data sets.

3.2 Abstraction Reactions

For a chemical reaction the required sequence of calls is considerably more complicated than for a molecular species. Furthermore, there are many different levels of approximation that could be used in estimating the rate constants. Low-level approximations are useful in performing survey studies over large sets of reactions to explore which reactions might be important. Meanwhile, calculations incorporating many different high-level components can yield the predictive accuracy required for improving the fidelity of a mechanism, but require significantly more CPU resources. The modular nature of EStokTP allows for the implementation of a multitude of different approximations for the rate constants. Importantly, the data produced by the different modules are readily reused as one considers alternative approaches for predicting the rate constants.

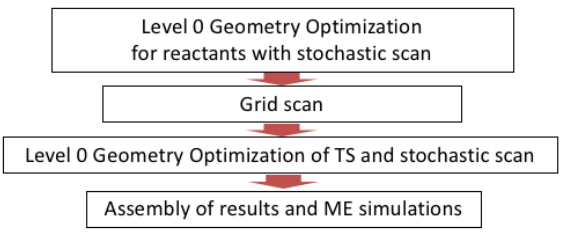

a)

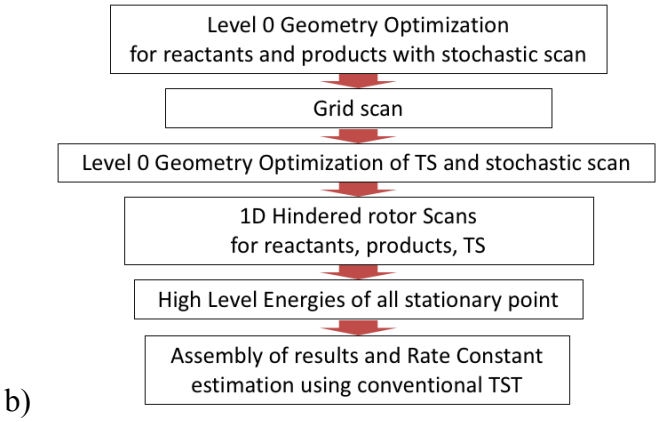

b)

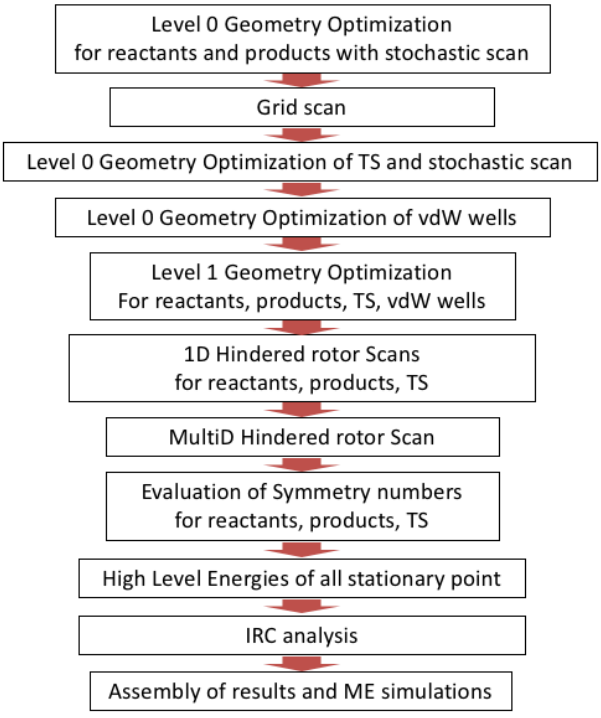

c)

Figure 8. Three possible sequences of EStokTP modules that could be used to determine rate constants for abstraction reactions: a) The minimum number of modules necessary for a low level rate constant estimate; b) A set of modules that can reproduce typical literature results; c) A set of modules that can yield highly accurate rate constant predictions.

In Fig. 8 we illustrate the sequence of calls required for a simplistic approach (8a), a common literature approach (8b), and a high level approach that we have found useful for predictive calculations (8c). A rate calculation will often be preceded by separate calculations for the two reactants (e.g., for the purpose of thermochemical property evaluations). The modular nature of

EStokTP allows for the ME blocks generated in the calculations of the molecular properties to be imported into the EStokTP directory for the rate evaluation, which allows the user to avoid repeating these calculations. In this instance, the low level approach simply requires a grid scan to find a first order approximation to the TS, followed by a formal transition state search, and then a Monte Carlo TS conformer search. Such low-level RRHO based approximations have a long history in the literature, although nowadays most published studies also include some form of hindered rotor correction and high-level energy analysis. The latter calculations simply require calls to two more modules of EStokTP, as in the scheme of Fig. 8b.

The set of calculations required for a high-accuracy prediction of the rate constant is significantly larger than those needed for low-level calculations. Again, the modular nature of EStokTP allows for the high level scheme to be initiated at the point where the low level scheme ended, assuming those calculations have already been completed. Similarly, EStokTP can simply import the TS structure found using an alternative search algorithm and then proceed from there through the desired sequential module call. The conversion from the TS output from some other code to that appropriate for EStokTP can readily be accomplished with the companion x2z geometry conversion utility.[40] The level 0 calculations should be followed by level 1 calculations, torsional scans, high level energy evaluations, and symmetry determinations for the TS as well as the reactants and products involved in the reaction.

For the vdW wells, hindered rotor scans, the stochastic search for conformational minima, as well as the determination of symmetry numbers are not included in the sequence of calculations reported in Fig. 8c. Accurately determining the density of states for vdW wells is difficult due to the many highly anharmonic low frequency vibrations that characterize the interaction between the two molecular fragments forming the vdW well, and the presence of multiple minima. Furthermore, as discussed in Sec. 2.9.1, the vdW wells are incorporated in the EStokTP analysis primarily to correctly estimate the barrier height for the calculation of tunneling coefficients. This aspect of the

analysis does not require a refined estimation of the density of states of the well, but just a high level determination of the ground energy.

It is instructive to consider the variation in the predicted rate constant with growing level of theory for the H-abstraction reaction of methylacetate by OH. This reaction is well suited to test the performance of EStokTP because it is characterized by the presence of multiple conformers, both for the reactant and the TS (cf. Fig. 9), by coupled HRs including the presence of H-bonds for some of the TS structures, and by the formation of a quite stable vdW well in the entrance channel. Furthermore, high quality experimental data are available for this reaction at both low and high temperatures.

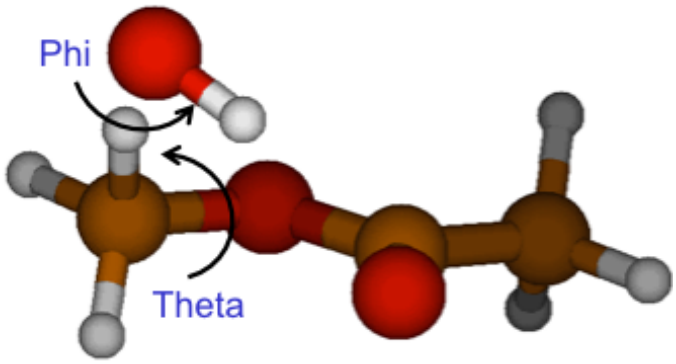

a)

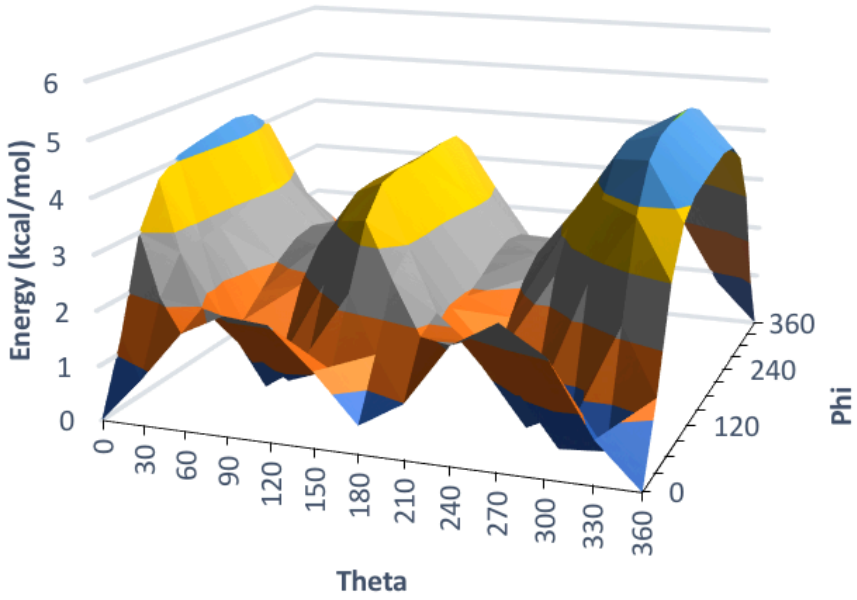

b)

Figure 9. Plot of the 2D (in phi and theta) torsional potential for the TS in the H-abstraction by OH from one of the methyl rotors in $CH_3C(O)OCH_3$.

The TS structure was determined using a grid scan along the coordinate set schematized in Fig. 3. A three TS model was used to construct the PES and to determine the reaction rates. The rate constants calculated at different levels of theory are compared in Fig. 10.

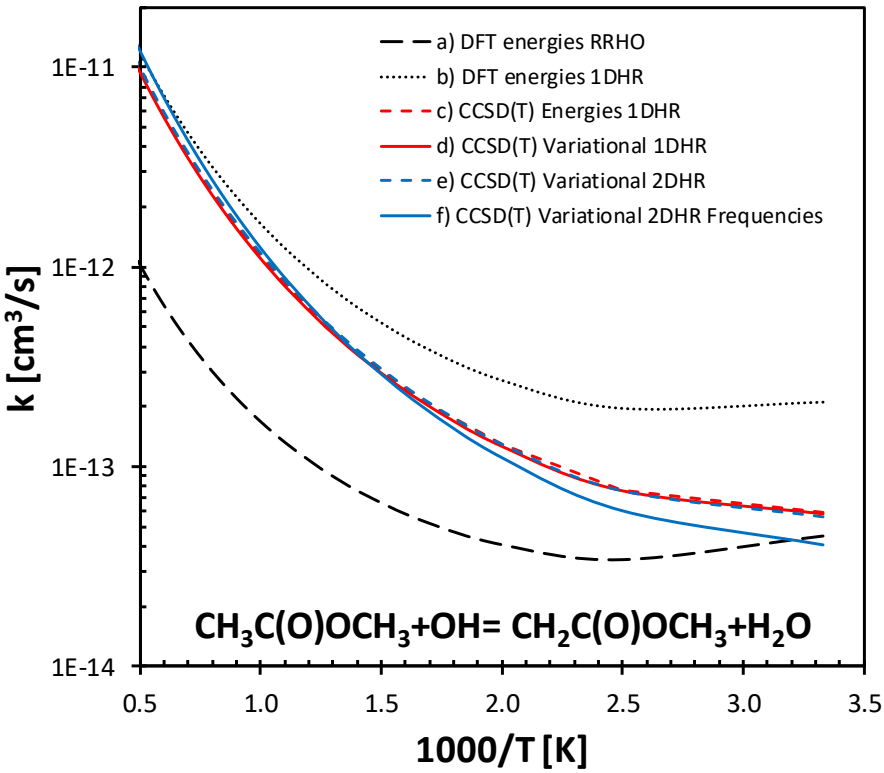

Figure 10. Impact of using increasing levels of theory for the calculation of the rate constant for H-abstraction from methyl acetate: $CH_3C(O)OCH_3 + OH \rightarrow CH_2C(O)OCH_3 + H_2O$. See the text for a description of computational methodologies a)-f).

The rate constants reported in Fig. 10 were determined: a) using DFT with the M06-2X functional and the aug-cc-pVTZ basis set to determine energies and vibrational frequencies of reactants, transitions states, vdW wells, and products, the RRHO approximation, and conventional TST (DFT energies RRHO); b) same as a) but using the 1D HR approximation for 4 torsional motions and

Hessian projection (DFT energies 1DHR); c) same as b) but using CCSD(T) energies extrapolated to the CBS limit; d) same as c), but using variational rather than conventional TST; e) same as d) but using a 2D Hindered rotor model for two HRs; f) same as e) but computing the Hessian for each point of the 2D scan and convoluting the vibrational density of states so determined with those of the HRs to determine the TS number of states. Quantum tunneling contributions determined using the Eckart model were included in all calculations.

The choice of the computational methodology used is seen to have a significant impact on the predicted rate constant. With method f) as a reference, the rate predictions based on DFT energies, the RRHO approximation and conventional TST differ by up to a factor of 10, especially at high temperatures. Using the 1D HR approximation for all relevant torsions considerably improves the predictions at high temperatures, while low temperatures estimates are then off by a factor of 4. This difference is largely due to the different energy barriers determined with DFT and CCSD(T) theories: 2.02 vs 2.75 kcal/mol. Using variational TST (d) and 2D HRs (e) has small impacts on the rate constant, while including the estimation of Hessians along the 2D PES scan had a small but not negligible effect.

The impact of the different computational methodologies can be better appreciated by comparing the predictions for the total H-abstraction rate with literature experimental data (Fig. 11). The comparison shows that the highest level computational methodology that is possible with EStokTP for abstraction reactions, which is the one outlined in Fig. 8c, reproduces experimental data to within a factor of 1.5, while 1DHR and 2DHR approaches underestimate the experimental values by a factor of 2. This discussion should not be interpreted as a general criticism of DFT, as DFT predictions are dependent on the choice of the functional and it is quite possible that using a functional more suitable to study the present reaction better results may be obtained. The main purpose of these calculations is to show that using the protocols implemented in EStokTP it is possible to systematically approach the experimental measurements, which is one of the two main

aims of EStokTP. This does not preclude an alternative approach, for example one based on a careful choice of DFT functionals for each portion of the calculation, reaching the same aim.

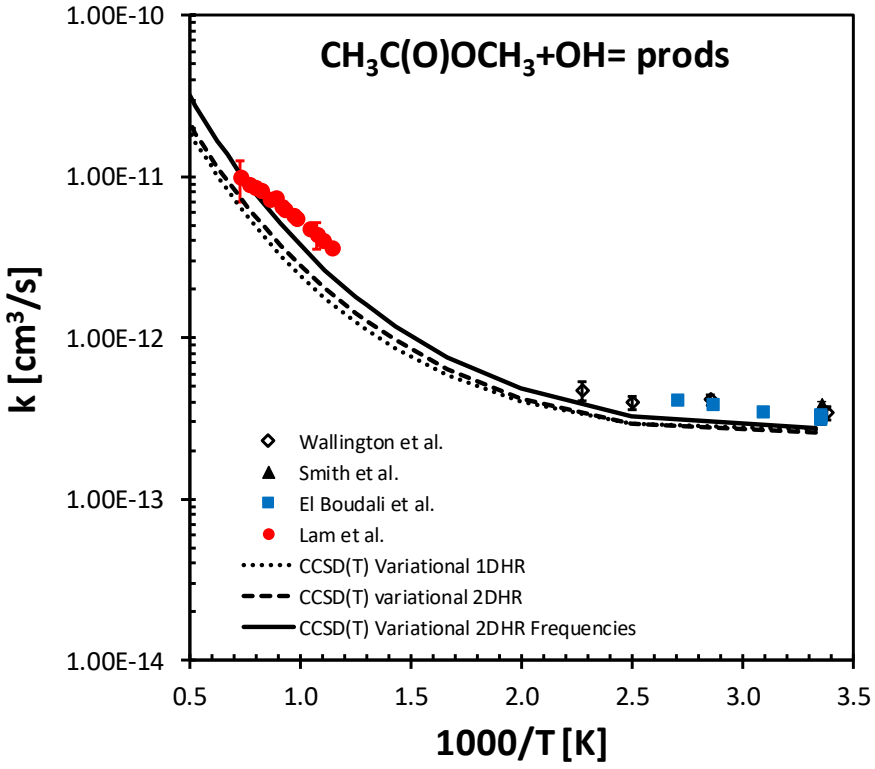

Figure 11. Comparison between theoretical predictions[42] and experimental measurements[71-73] of the rate constant for H-abstraction by OH from both methyl groups in $CH_3C(O)OCH_3$.

The second aim for EStokTP is to be able to determine rate constants automatically, once the input files have been properly set up. For this purpose, two sets of extensive tests have been performed for abstraction reactions to determine the probability of success of the algorithms implemented in EStokTP for each module. At present there is in fact considerable interest in being able to perform calculations automatically for large sets of reactions, but there is no benchmark to check how an automatic algorithm performs. The whole purpose of these calculations is to provide such benchmark.

In the first test set the rate of H-abstraction from 11 species by 5 different radicals has been determined using the computational protocol shown in Fig. 8c, only excluding the multidimensional HR treatment. The considered species are CH_4, C_2H_6, C_2H_4, C_2H_2, CH_3OH, $HC(O)OH$, CH_3OCH_3,

H_2CO, CH_3Cl, H_2S, and NH_3. The abstracting radicals are H, OH, OOH, CH_3, and O, which are typically of importance in combustion chemistry. A total of 65 reactions are considered, as HC(O)OH and CH_3OH have two non-equivalent hydrogens. This test set was named HAB65.

The simulations were organized as follows. First, separate calculations were performed for each of the reactants and products using the protocol shown in Fig. 7 and ME blocks were generated for each of these species. Then, input files were generated for each reaction using a wrapper script that automatically accounts for the possibility that each one of these specific radicals has internal rotors at the TS. The following computational protocol was used: level 0: M06-2X/6-31+G(d,p); level 1 and IRC: M06-2X/aug-cc-pVTZ; hindered rotor scans and symmetry: M06-2X/6-311+G(d,p); high level calculations: CCSD(T)/aug-cc-pVTZ with CBS basis set correction given by DF-MP2/aug-cc-pVQZ - DF-MP2/aug-cc-pVTZ. TS searches were performed in internal coordinates, computing the Hessians only for the first structure. All DFT calculations were performed using G09 and all CCSD(T) and DF-MP2 calculations were performed with Molpro 2010. The 65 simulations were then submitted to a queue manager on an HPC Linux cluster. The simulation results are summarized in Table 1.

Table 1. Summary of the performance of the EStokTP algorithms for a test set of 65 abstraction reactions (HAB65).[a]

Reaction[b]	TS	W	HR	HL	V	S	k (300 K)[c]	k (1000 K)[c]
CH_4 + H	y	y	y	y	y	y	5.2E-19	3.8E-13 (2.9E-13)[74]
+ OH	y	y	y	y	y	n[d]	5.1E-15 (7.0E-15)[75]	2.0E-12 (1.7E-12)[75]
+ OOH	y	y	y	y	y	y	3.1E-28	1.0E-16 (7.7E-17)[76]
+ CH_3	y	y	y	y	y	y	1.4E-32	9.0E-16
+ O	y	y	y	y	y	y	1.2E-17	6.2E-13 (7.0E-13)[77]
C_2H_6 + H	y	y	y	y	y	y	8.8E-17 (7.5E-17)[78]	2.6E-12 (2.2E-12)[78]
+ OH	y	y	y	y	y	y	3.4E-13 (2.81E-13)[79]	1.1E-11 (8.7E-12)[79]
+ OOH	y	c[p]	y	y	y	y	7.4E-25	1.7E-15
+ CH_3	y	y	y	y	y	n	3.0E-21	9.8E-15
+ O	y	y	y	y	y	y	1.1E-15	3.6E-12 (4.2E-12)[77]
C_2H_4 + H	y	y	y	y	y	y	1.3E-20	2.0E-13
+ OH	y	y	y	y	y	y	5.6E-15	2.1E-12 (2.1E-12)[80]
+ OOH	y	y	y	y	y	y	3.1E-30	3.3E-17
+ CH_3	y	y	y	y	y	y	7.6E-24	1.6E-15
+ O	y	y	y	n[w]	y	y	7.4E-19	4.5E-13
C_2H_2 + H	y	y	y	y	y	y	8.5E-33 (1.4E-32)[81]	2.0E-17

+ OH	y	b[p]	y	y	y	y	3.7E-24	7.9E-15
+ OOH	y	y	y	y	y	y	1.0E-45	1.8E-21
+ CH_3	y	c[p]	y	y	y	y	5.8E-33	4.4E-18
+ O	n							
C**H**$_3$OH + H	y	y	y	y	y	Y	8.0E-16	2.1E-12
+ OH	y	y	y	y	y	y	5.8E-13	5.4E-12
+ OOH	y	y	y	y	y	y	2.6E-23	5.1E-16
+ CH_3	y	y	y	y	y	y	3.3E-20	8.4E-15
+ O	y	n[p]	y	y	y	y	3.1E-15	2.8E-12 (2.2E-12)[82]
CH_3O**H** + H	y	y	y	y	y	y	1.2E-19	7.1E-14
+ OH	y	b[p]	y	y	y	y	1.3E-13	7.4E-13
+ OOH	y	y	y	y	y	y	4.2E-27	5.6E-17
+ CH_3	y	b[p]	y	y	y	y	9.6E-21	2.5E-15
+ O	y	n[p]	y	y	y	y	4.5E-18	6.9E-14
HC(O)OH + H	y	y	y	y	y	y	4.5E-17	5.6E-13
+ OH	y	b[p]	y	y	y	y	3.9E-15	6.2E-13
+ OOH	y	b[p]	y	y	y	y	7.5E-25	8.6E-17
+ CH_3	y	c[p]	y	y	y	y	6.1E-20	1.1E-14
+ O	y	y	y	y	y	y	1.3E-17	1.6E-13
HC(O)O**H** + H	y	n[p]	y	y	y	y	1.2E-23	1.1E-14
+ OH	y	y	y	y	y	y	1.2E-14	5.8E-14
+ OOH	y	y	y	y	y	y	1.1E-34	2.7E-21
+ CH_3	y	b[p]	y	y	y	y	1.1E-23	6.3E-16
+ O	y	y	y	n[w]	y	y	7.5E-25	3.7E-15
CH_3OCH_3 + H	y	b[p]	y	y	y	y	3.5E-15 (5.6E-15)	5.0E-12 (6.6E-12)[83]
+ OH	y	b[p]	y	y	y	y	3.9E-12 (2.9E-12)[84]	1.5E-11 (2.4E-11)[85]
+ OOH	y	y	y	y	y	y	6.4E-23	2.1E-15
+ CH_3	y	y	y	y	y	y	8.2E-20	2.4E-14
+ O	y	y	y	y	y	y	2.9E-14 (6.6E-14)[86]	1.6E-11 (1.1E-11)[87]
$H_2C(O)$ + H	y	b[p]	y	y	y	y	8.7E-14 (4.3E-14)[88]	9.7E-12
+ OH	y	y	y	y	y	y	1.3E-11	1.9E-11 (2.0E-11) [89]
+ OOH	y	y	y	y	y	y	5.2E-20	7.9E-15
+ CH_3	y	y	y	y	y	y	1.8E-17	8.4E-14
+ O	y	y	y	y	y	y	4.0E-14	9.0E-12
CH_3Cl + H	y	y	y	y	y	y	2.0E-17	7.5E-13
+ OH	y	b[p]	y	y	y	y	5.9E-14 (3.7E-14)[90]	3.1E-12
+ OOH	y	y	y	y	y	y	3.2E-26	1.5E-16
+ CH_3	y	y	y	y	y	y	1.2E-20	1.3E-14
+ O	y	b[p]	y	y	y	y	6.9E-17	7.4E-13 (7.9E-13)[91]
H_2S + H	y	b[p]	y	y	y	y	1.3E-12 (9.6E-13)[92]	2.9E-11 (2.8E-11)[92]
+ OH	y	y	y	y	y	y	5.7E-12 (5.3E-12)[93]	1.3E-11
+ OOH	y	b[p]	y	y	y	y	3.9E-21	7.5E-15
+ CH_3	y	b[p]	y	y	y	y	1.7E-14	7.9E-13
+ O	y	y	y	n[w]	y	y	2.9E-54	5.8E-24
NH_3 + H	y	b[p]	y	y	y	y	3.0E-19	1.7E-13(9.4E-14)[94,95]
+ OH	y	y	y	y	y	y	1.6E-13 (1.5E-13)[96]	3.2E-12 (3.2E-12)[97]
+ OOH	y	y	y	y	y	y	1.9E-27	1.1E-16
+ CH_3	y	b[p]	y	y	y	y	6.4E-22	3.6E-15
+ O	y	y	y	n[w]	y	y	1.7E-18	1.8E-13 (3.9E-13)[98]

[a] The acronyms have the following meanings: TS (y/n), the transition state was/was not found; HR, the hindered rotor scan was/was not successful; HL, high level calculations were/were not successful; S, the correct global symmetry factor was/was not found; W, vdW wells were/were not found; V, variational calculations were/were not successful; b indicates that the vdW well on the

product side has one or more imaginary frequencies; c indicates that locating the vdW well on the product side required a tuning of the optimization parameter.
[b] The bold atom denotes the site of the abstraction.
[c] Rate constants calculated for the 3TS model are reported in cm^3 $molecule^{-1}$ s^{-1} at 300 and 1000 K and compared with a selection of experimental data (in parentheses). This comparison is meant to be representative of reasonably established values, rather than exhaustive.
[d] The symmetry factor is off by a factor of 7/6.
[p] Refers to the product side of the PES.
[w] Refers to the well.

A statistical analysis of the HAB65 test set results is promising. The abstraction algorithm succeeded in finding a TS in 98% of the cases, with the only failure for the $O(^3P) + C_2H_2$ reaction, which is highly endothermic (30 kcal/mol) and may well be barrierless in the reverse direction. This means that in all other cases it would have been possible to obtain a reasonable first approximation to the rate constant using RRHO assumptions and the protocol shown in Fig. 8a. IRC scans and 1D HR calculations were always successful. The latter in particular is reassuring as it is possible that an HR scan for a TS may lead to TS structures that connect different minima than those from the reference TS geometry. This success indicates that the adopted algorithm and the implemented fall back options are quite effective. The symmetry algorithm also worked nicely with only a minor failure, which leads to an overestimation of the correct value by a factor of 7/6, and a main failure, leading to an error of a factor of 2, where the optical symmetry number was erroneously assigned a value of 2. In reality the two enantiomers are essentially the same because the barrier for interconversion is negligible and the torsional angle that separates them is quite small.

In several (15) cases the vdW wells had 1 or more imaginary frequencies. This is not considered problematic because the vdW frequencies are not used in the rate constant estimation procedure, except in the estimation of zero point energies (ZPEs) and, probably, positive (though quite likely very small) values could be obtained by tightening the convergence criteria. What is more troubling is that in 4 cases the calculation of high level energies for the vdW wells failed. This failure was always due to the lack of convergence in the solution of the restricted spin Hartree Fock equations, which is likely related to the presence of nearly degenerate states for species like OH interacting

with a closed shell molecule at large separations. This failure is troubling because it halts progress for the EStokTP algorithm so that a rate constant cannot be automatically determined. This limits the success in the automatic determination of rate constants to 93 %.

Two workarounds are possible. The first is to organize the automatic determination of the rate constants so that evaluations are performed at increasing levels of theory as these become available. For example, downgrading the rate constant estimation protocol from 3TS to 2TS (see Fig. 5 and the related discussion) would increase the overall success rate for the rate constant determinations to 98%. The second is to devise fall back options for situations where ROHF fails. Finally, it is nice to observe that the correct global symmetry number was determined in 97% of the investigated systems, thus indicating that the symmetry algorithm is reasonably stable.

In order to further check the performance of the EStokTP algorithms and protocols a second test set was considered. This set is composed of H-abstractions from all the molecules in the HAB65 test set by the radicals C_2H, C_2H_3, C_2H_5, Cl, HS, NH_2, and $^3O_2$. This test set comprises 91 reactions and was named HAB91. The HAB65 set was designed to test the accuracy and success rate of the present automatic rate constant determination algorithms for reactions representative of those that are likely to play an important role in combustion and for which experimental data are commonly available. Meanwhile, the HAB91 set provides a more challenging set of systems to describe. For example, reactions with C_2H_5 have a large number of HRs in the TS. Abstraction by C_2H is challenging as it is difficult to define a set of coordinates for molecular systems that are in part linear that does not lead to problems in geometry optimizations. Furthermore, the HAB91 test set includes atoms of the second row (Cl and S), so that the impact of d orbitals on finding geometries of stationary points can be investigated. Also, determining TSs for O_2 abstraction is often quite challenging because it is a significantly endothermic process. For this reason, the $^3O_2$ reactions were actually studied in the reverse direction (cf. Sec. 2.1), i.e., as abstractions of an H from HO_2. However, in this direction the reactions are effectively barrierless, which also creates some troubles

for the algorithm. NH_2 and C_2H_3 are included in the test set to investigate whether nitrogen and planar radicals pose a challenge to the EStokTP algorithms. The simulation results are summarized in Table 2.

Table 2. Summary of the performance of EStokTP for a test set of 91 abstraction reactions (HAB91).[a]

Reaction[b]	TS	W	HR	HL	V	S	k (300 K)[c]	k (1000 K)[c]
CH_4 + C_2H	y	y	y	y	y	y	4.4E-12 (3.09E-12)[99]	1.3E-11
+ C_2H_3	y	y	y	y	y	y	1.0E-19	2.2E-14
+ C_2H_5	y	y	y	y	y	y	2.2E-24	6.9E-16
+ Cl	y	y	y	y	y	y	9.9E-14(1.1E-13)[100]	1.4E-11(9.3E-12)[100]
+ HS	y	n[p]	y	y	y	n[d]	2.9E-23	1.5E-14
+ NH_2	y	y	y	y	y	y	4.0E-20(1.9E-20)[101]	2.0E-14 (1.3E-14)[102]
+ O_2	y	y	y	y	y	y	2.0E-50	2.8E-22
C_2H_6 + C_2H	y	y	y	y	y	y	4.1E-11(3.8E-11)[103]	3.41E-11
+ C_2H_3	y	y	y	y	y	y	6.6E-18	8.2E-14
+ C_2H_5	y	y	y	y	y	y	1.3E-22	2.5E-15
+ Cl	y	y	y	y	y	y	8.6E-11(5.7E-11)[104]	6.3E-11(1.2E-10)[105]
+ HS	y	y	y	y	y	y	4.2E-20	1.5E-13
+ NH_2	y	y	y	y	y	n	4.7E-18 (3.8E-18)[101]	1.2E-13
+ O_2	y	y	y	y	y	y	5.7E-47	3.4E-21
C_2H_4 + C_2H	y	n[r,p]	y	y	y	y	4.3E-12	1.6E-11
+ C_2H_3	y	y	y	y	y	y	1.7E-20	7.8E-15
+ C_2H_5	y	y	y	y	y	y	4.6E-25	3.8E-16
+ Cl	y	n[r]	y	y	y	y	6.2E-15(1.56E-15)[106]	1.2E-11
+ HS	y	y	y	y	y	y	9.1E-26	3.4E-15
+ NH_2	y	y	y	y	y	y	1.1E-20	1.8E-14
+ O_2	y	y	y	y	y	y	9.4E-54	5.1E-23
C_2H_2 + C_2H	y	y	y	y	y	y	7.4E-19	1.7E-14
+ C_2H_3	y	y	y	y	y	y	1.1E-18	7.3E-17
+ C_2H_5	y	y	y	y	y	y	4.8E-15	8.4E-19
+ Cl	y	y	y	y	y	y	5.6E-26	6.9E-17
+ HS	y	y	y	y	y	y	2.5E-40	3.2E-19
+ NH_2	y	y	y	y	y	y	1.7E-29	1.4E-16
+ O_2	n[i]							
C**H**$_3$OH + C_2H	y	y	y	y	y	y	7.2E-12	1.0E-11
+ C_2H_3	y	y	y	y	y	y	2.9E-17	8.5E-14
+ C_2H_5	y	y	y	y	y	y	1.0E-21	1.8E-15
+ Cl	y	y[g,r]	y	y	y	y	3.4E-11 (5.8E-11)[107]	4.8E-11
+ HS	y	y	y	y	y	y	5.7E-18	3.2E-13
+ NH_2	y	y	y	y	y	y	2.3E-17	8.6E-14
+ O_2	y	y	y	y	y	y	8.4E-45	1.6E-21
CH_3O**H** + C_2H	y	y	y	y	y	n[f]	9.1E-13	6.4E-12
+ C_2H_3	y	y	y	y	y	y	8.6E-17	1.0E-13
+ C_2H_5	y	y	y	y	y	y	5.4E-22	8.8E-16
+ Cl	y	y	y	y	y	y	2.5E-13	3.0E-12
+ HS	y	y	y	n[TS]	y	y		

+ NH_2	y	y	y	y	y	y	1.4E-17	3.2E-14
+ O_2	y	y	y	n[z]	y	y		
HC(O)OH + C_2H	y	y	y	y	y	y	9.3E-13	2.9E-12
+ C_2H_3	y	y	y	y	y	y	1.8E-17	3.8E-14
+ C_2H_5	y	y	y	y	y	y	3.3E-21	2.4E-15
+ Cl	n[h]	y	y	y	y	y	4.3E-12	6.2E-12
+ HS	y	y	y	y	y	y	6.4E-21	1.8E-14
+ NH_2	y	y	y	y	y	y	1.2E-18	1.5E-14
+ O_2	y[h]	y	y	y	y	y	3.3E-26	3.2E-22
HC(O)O**H** + C_2H	y	y	n[k]	y	y	y	3.9E-12	6.7E-13
+ C_2H_3	y	y	y	y	y	y	3.6E-20	7.0E-15
+ C_2H_5	y	y	y	y	y	y	8.3E-25	1.4E-16
+ Cl	y	y	y	y	y	y	2.0E-13	5.3E-14
+ HS	y	y	y	y	y	y	3.1E-26	8.1E-17
+ NH_2	y	y	y	y	y	y	2.6E-17	3.7E-14
+ O_2	n							
CH_3OCH_3 + C_2H	y	n[r,p]	y	y	y	y	4.0E-11	2.0E-11
+C_2H_3	y	y	y	y	y	y	1.2E-16	3.3E-13
+C_2H_5	y	y	y	y	y	y	5.0E-21	1.2E-14
+Cl	n[l]	y	y	y	y	y	1.30E-6	9.2E-10
+HS	n[m]	y	y	y	y	y	1.0E-16	2.7E-12
+NH_2	y	y	y	y	y	y	4.9E-17	1.7E-13
+O_2	y	y	y	y	y	y	8.4E-44	1.7E-20
$H_2C(O)$ + C_2H	y	y	y	y	y	y	1.7E-11	2.2E-11
+C_2H_3	y	y	y	y	y	y	3.7E-15	4.5E-13
+C_2H_5	y	y	y	y	y	y	3.1E-18	3.7E-14
+ Cl	n							
+ HS	y	y	y	y	y	y	1.1E-14	3.4E-12
+ NH_2	y	y	y	y	y	y	2.2E-15	5.8E-13
+ O_2	y	y	y	y	y	y	2.1E-40	4.0E-20 (1.1E-19)[108]
CH_3Cl+C_2H	y	y	y	y	y	y	5.3E-12	8.7E-12
+C_2H_3	y	y	y	y	y	y	8.0E-18	4.1E-14
+C_2H_5	y	y	y	y	y	y	6.8E-22	2.5E-15
+Cl	y	y	y	y	y	y	1.1E-12(5.3E-13)[109]	9.0E-12
+HS	y	y	y	n[o]	y	y	2.0E-21	3.1E-14
+NH_2	y	y	y	y	y	n	9.5E-18	1.8E-13
+ O_2	y	y	y	y	y	y	3.4E-48	5.2E-22
H_2S + C_2H	y	y	y	y	y	y	1.4E-10	8.7E-11
+ C_2H_3	y	y	y	y	y	y	1.2E-12	3.6E-12
+ C_2H_5	n[n]	y	y	y	y	y	1.4E-14	3.6E-13
+ Cl	y	y	y	y	y	y	2.3E-16	2.8E-13
+ HS	y	y	y	y	y	y	2.4E-15	1.1E-12
+ NH_2	y	y	y	y	y	y	1.3E-13	2.5E-12
+ O_2	y	y	y	y	y	n[e]	5.4E-41	7.8E-20
NH_3 + C_2H	y	y	y	y	y	y	7.6E-11	3.5E-11
+ C_2H_3	y	y	y	y	y	n[e]	2.4E-18	4.8E-14
+ C_2H_5	y	y	y	y	y	y	2.6E-23	7.9E-16
+ Cl	y	n[p]	y	y	y	y	1.9E-13(1.09E-13)[110]	1.2E-11
+ HS	y	y	y	y	y	y	1.5E-24	3.4E-15
+ NH_2	y	y	y	y	y	y	1.6E-19	8.8E-15
+ O_2	n							

[a] The acronyms have the same meanings as in Table 1, i.e.; TS (y/n), the transition state was/was not found; HR, the hindered rotor scan was/was not successful; HL, high level calculations were/were not successful; S, the correct global symmetry factor was/was not found; W, vdW wells were/were not found; V, variational calculations were/were not successful.
[b] The bold atom denotes the site of the abstraction.
[c] Rate constants calculated for the 3TS model are reported in cm^3 $molecule^{-1}$ s^{-1} at 300 and 1000 K and compared with a selection of experimental data (in parentheses). This comparison is meant to be representative of reasonably established values, rather than exhaustive.
[d] The symmetry factor is off by a factor of 5/6.
[e] The symmetry factor is off by a factor of 2.
[f] The symmetry factor is off by a factor of 3.
[g] The energy of the reactant vdW well is higher than that of the TS when computed at the CCSD(T) level but not at the DFT level.
[h] A lower energy conformational isomer for the TS was missed in the first stochastic scan, but was found in a second scan with an increased number of stochastic points.
[i] The TS was not found with the default optimization options, but could be found by computing the Hessians at each optimization point.
[j] The determined TS failed as it converged to the wrong structure (the HR energy barriers were quite high for this system).
[k] The HR scan for the TS failed as it converged to the wrong structure.
[l] The TS energy barrier is significantly below the reactants energy; a VTST analysis for the entrance channel would be needed for a proper description.
[m] The TS is sensitive to the initial H-abstraction choice.
[n] The minimum energy TS structure was not found using the default number of stochastic points.
[o] The high level energy for the TS has a high (0.05) T1 diagnostic.
[p] Refers to the product side of the PES.
[r] Refers to the reactant side of the PES.
[w] Refers to the well.
[z] The determined TS does not connect the desired reactants and products.

Although more errors were observed for the HAB91 test set, the performance of EStokTP is still very encouraging. Transition states were found for 94% of the reactions, though only 92% were absolute minima. Notably four out of the seven cases in which the TS was not found involve O_2 as a reactant, which is a particularly difficult system to study, as mentioned above. The single failure found for the HR algorithm is for a case where the torsional barrier is higher than 10 kcal/mol. The algorithm we use to setup the data files probably should not have treated this torsion as a hindered rotor. The symmetry algorithm succeeds in only 93.5% of the cases, which is somewhat worrisome as it will affect the average accuracy of the computed rate constants. In 5% of the cases it was not possible to find the reactant or product vdW well. On the whole, it is reasonable to conclude that the EStokTP protocols were also reasonably successful for the HAB91 test set. Continued efforts, such

as properly incorporating an automated VTST reaction rate algorithm for barrierless reactions, will further reduce the errors.

Finally, it is possible to draw some conclusion on the accuracy of the present calculations for the 22 reactions for which well assessed experimental data are available comparing the calculated and experimental rate constants. The mean unsigned errors of the common logarithms of the rate constants at 300 and 1000 K are 0.19 and 0.16, respectively. The increase of uncertainty going from high to low temperature rate constants could be reasonably expected and it likely reflects the uncertainties in the calculated energy barriers. Considering that a mean unsigned error of 0.3 is a factor of 2 in the theoretical to experimental rate constant ratio for both overestimates and underestimates, it can be noted that in both cases the agreement with respect to experiments is quite good, even if the level of theory used for the calculations is not what would be the state of the art for such small molecules. It should be noted that it is reasonable to expect larger uncertainties for abstraction reactions when larger molecules, with several coupled internal degrees of freedom are studied, as is the case for the $CH_3C(O)OCH_3$ + OH abstraction reactions discussed above.

In addition to the benchmark tests discussed here, it should be noted that EStokTP has already been successfully utilized to obtain high accuracy predictions for H-abstraction rate constants in acetic acid,[111] toluene,[2] and methyl and ethyl acetate oxidation.[42]

3.3 Addition

Several protocols are also possible for determining addition rate constants. The complete abstraction protocol shown in Fig. 8c) can be replicated for addition reactions, except for the vdW well on the product side, which does not exist for addition reactions. Alternatively, it is possible to use the EStokTP algorithm for finding vdW wells to discover the structure of the chemically bound product complex. The advantage of this protocol, shown in Fig. 12, is that there is no need to know or determine a priori the structure of the reaction products. However, this protocol may occasionally lead to some product conformer other than the minimum energy conformer.

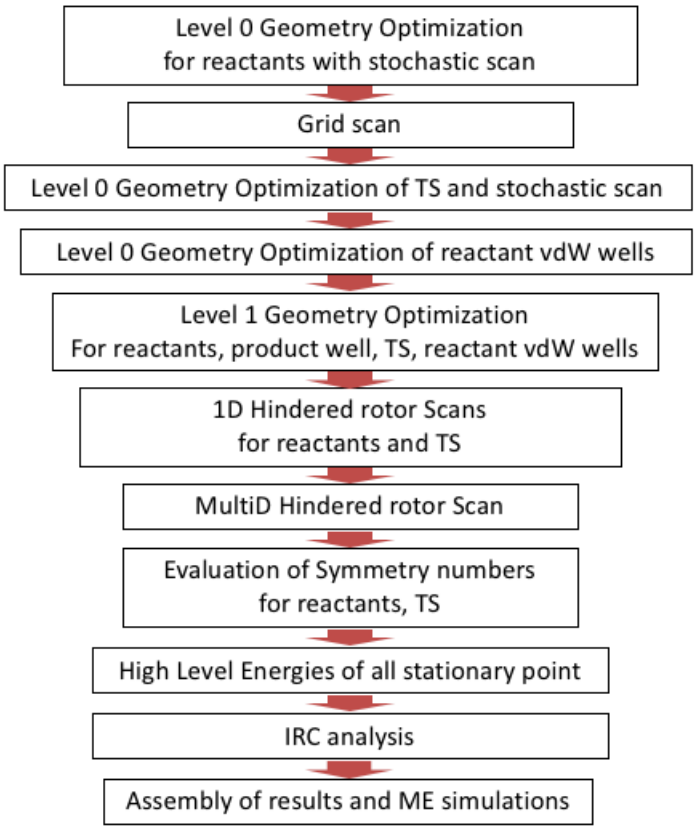

Figure 12. A sequence of EStokTP modules for determining addition rate constants for reactions. With this protocol, the geometry of the product is determined automatically using the same algorithm that is generally used for determining the product vdW well.

The protocol shown in Fig. 12 was used to study the addition of H atoms to C_2H_4. This is a reaction that has been extensively studied in the literature, both experimentally[112] and theoretically.[113,114] Here, calculations were performed at the same theoretical level used to study the rate constant for H-abstraction from methyl acetate (see section 3.2) by OH. The rate constants for addition reactions are characterized by a significant pressure dependence, as evidenced in Fig. 13. The coupled EStokTP and MESS codes are suitable for studying pressure dependent reactions. The only additional requirement for the user is to supply an estimate of the collisional energy transfer parameters.

The simulations reported in Fig. 13 were performed using literature Lennard-Jones parameters for He and C_2H_5 (the C_2H_6 parameters were used in this case) and the ΔE_{down} temperature dependent

expression recommended by Miller and Klippenstein.[114] For this specific reaction, tunneling corrections were determined at the HPL level also using SCT theory, as implemented in EStokTP. A hundred steps were taken in the reactant and product directions from the saddle points using a step of 0.02 bohr. Hessians were computed at each point along the PES. It can be noted how, also in this case, increasing the level of theory leads to an improved agreement with experimental data.

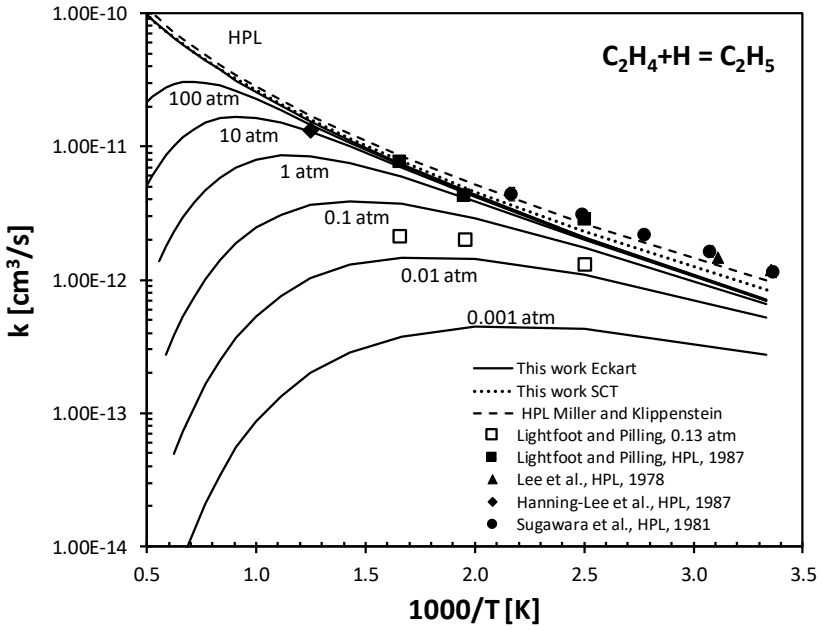

Figure 13. Comparison of the rate constant calculated for H addition to C_2H_4 with literature values.[114-118] The pressure dependence was predicted by solving the 1D master equation for an exponential down energy transfer model. Simulations were performed for a He bath gas.

For addition reactions, we performed a statistical analysis of the success rate of the EStokTP algorithms in similar fashion to what was done for abstraction reactions. In particular, the same two sets of abstracting radicals considered in the HAB65 and HAB91 reaction sets were added to four different molecules: C_2H_2, C_2H_4, HC(O)OH, and H_2CO. Two different addition centers were considered for formic acid and formaldehyde, so that the total number of reactions investigated for the first set is 30 (ADD30), while for the second is 42 (ADD42). Calculations were performed at the

same level of theory used to study the abstraction reactions (see above) for the RRHO 1D HR model and variational TST analyses. Rate constants were determined using the 2TS model discussed in section 2.9.2.

The simulation results are summarized in Table 3 and Table 4. Notably, as is sometimes the case when trying to construct reaction sets without using chemical knowledge on a case by case basis, some of the investigated reactions lead to products that are either very shallow wells or that, in several cases, are not a PES minimum as there is no energy barrier to their separation to products. This is the case for 2 reactions in the ADD30 set and for 5 reactions in the ADD42 set.

Table 3. Summary of the performance of EStokTP for a test set of 30 addition reactions (ADD30).[a]

Reaction[b]	TS	W	HR	HL	V	S	k (300 K)[c]	k (1000 K)[c]
C_2H_4 + H	y	y	y	y	y	y	7.1E-13 (1.1E-12)[119]	1.5E-11
+ OH	y	y	y	y	y	y	4.7E-12 (8.2E-12)[120]	5.8E-12
+ OOH	y	y	y[d]	y	y	y	3.2E-23	
+ CH_3	y	y	y	y	y	y	8.6E-19	3.0E-14
+ O	y	y	y	y	y	y	1.6E-13	3.4E-12
C_2H_2 + H	y	y	y	y	y	y	2.3E-13	3.5E-11 (3.0E-11)[121]
+ OH	y	y	y	y	y	y	4.1E-13 (8.7E-13)[122]	5.1E-12
+ OOH	y	y	y	y	y	y	1.2E-24	1.6E-15
+ CH_3	y	y	y	y	y	y	5.3E-19	6.8E-14
+ O	y	y	y	y	y	y	6.4E-14 (1.6E-13)[123]	7.2E-12 (1.2E-11)[124]
H**C**(O)OH + H	y	y	y	y	y	y	1.2E-18	1.3E-13
+ OH	y	y	y	y	y	y	3.3E-20	3.0E-15
+ OOH	y	y	y	y	y	y	3.5E-34	
+ CH_3	y	y	y	y	y	y	7.3E-24	1.4E-16
+ O	y	y	y	y	y	y	1.8E-23	8.8E-16
HC(**O**)OH + H	y	y	y	y	y	y	1.9E-20	3.3E-14
+ OH			Unst					
+ OOH			Unst					
+ CH_3	y	y	y	y	y	y	5.4E-33	6.5E-19
+ O	y	y	y	y	y	y	1.8E-23	8.8E-16
H_2**C**(O) + H	y	y	y	y	y	y	3.1E-14	2.5E-12
+ OH	y	y	n[e]	y	y	y	3.1E-33	9.5E-12
+ OOH	y	y	n[e]	y	y	y	1.9E-28	2.0E-18
+ CH_3	y	y	y	y	y	y	3.5E-18	1.4E-14
+ O	y	y	y	n	y	y		
H_2C(**O**) + H	y	y	y	y	y	y	9.5E-18	3.8E-13
+ OH	y	y	y	y	y	y	f	f
+ OOH	n							
+ CH_3	y	y	y	y	y	y	1.2E-26	8.5E-17
+ O	y	y	y	y	y	y	1.4E-32	6.1E-18

[a] The acronyms have the same meanings as in Table 1, i.e.; TS (y/n), the transition state was/was not found; HR, the hindered rotor scan was/was not successful; HL, high level calculations were/were not successful; S, the correct global symmetry factor was/was not found; W, wells and reactant vdW wells were/were not found; V, variational calculations were/were not successful; Unst denotes that the product is either a very shallow minimum or it is not a well on the PES.
[b] The bold atom denotes the site of the addition.
[c] Rate constants calculated for the 2TS model are reported in cm^3 $molecule^{-1}$ s^{-1} at 300 and 1000 K and compared with a selection of experimental data (in parentheses). This comparison is meant to be representative of reasonably established values, rather than exhaustive.
[d] To obtain converged results the HR backup options had to be modified, i.e., by imposing a search with a fixed R_{TS} rather than for a torsionally constrained saddle point.
[e] The automatically selected HR does not converge to the TS structure and was therefore treated as a HO.
[f] The product well energy is similar to that of the TS, so that a proper phenomenological rate constant does not exist.

Table 4. Summary of the performance of EStokTP for a test set of 42 addition reactions (ADD42).[a]

Reaction[b]	TS	W	HR	HL	V	S	k (300 K)[c]	k (1000 K)[c]
C_2H_4 + C_2H	n[d]							
+ C_2H_3	y	y	y	y	y	y	3.2E-16 (6E-16)[125]	1.5E-13
+ C_2H_5	y	y	y	y	y	y	6.7E-19	1.8E-14
+ Cl	n[d]							
+ HS	y	y	y	y	y	y	6.3E-13	3.3E-12
+ NH_2	y	y	y	y	y	y	1.0E-16	9.3E-14
+ O_2	y	y	y	y	y	y	e	e
C_2H_2 + C_2H	y	y	y	y	y	y	1.5E-10 (1.5E-10)[126]	6.6E-11
+ C_2H_3	y	y	y	y	y	y	1.5E-16 (2.9E-16)[127]	3.6E-13
+ C_2H_5	y	y	y	y	y	y	4.7E-19	4.3E-14
+ Cl	n[d]							
+ HS	y	y	y	y	y	y	3.5E-14 (3.3E-14)[128]	3.8E-12
+ NH_2	y	y	y	y	y	y	2.3E-17	1.4E-13
+ O_2	y	y	y	y	y	y		
H**C**(O)OH + C_2H	y	y	y	y	y	y	2.4E-17	3.8E-14
+ C_2H_3	y	y	y	y	y	y	1.5E-20	9.4E-16
+ C_2H_5	y	y	y	y	y	y	6.3E-23	
+ Cl	y	y	y	y	y	y	5.3E-22	1.9E-15
+ HS			Unst.					
+ NH_2	y	y	y	y	y	y	3.6E-22	3.2E-16
+ O_2	y	y	y	n	y	y		
HC(**O**)OH + C_2H	y	y	y	y	y	y	6.3E-15	3.2E-14
+ C_2H_3	y	y	y	y	y	y	3.1E-28	9.1E-18
+ C_2H_5	y	y	y	y	y	y	2.0E-31	1.5E-18
+ Cl			Unst.					
+ HS			Unst.					
+ NH_2	y	y	y	y	y	y	e	e
+ O_2			Unst.					
H_2**C**(O) + C_2H	y	n[r]	y	y	y	y	3.0E-14	6.3E-13
+ C_2H_3	y	y	y	y	y	y	9.5E-16	8.3E-14
+ C_2H_5	y	y	y	y	y	y	2.6E-17	1.4E-14
+ Cl	y	n[r]	y	y	y	y	9.4E-16	2.7E-13
+ HS	y	y	y	y	y	y	3.0E-18	1.5E-14

+ NH_2	y	y	y	y	y	y	1.5E-16	2.5E-14
+ O_2	y	y	y	n	y	y		
H_2C(**O**) + C_2H	y	y	y	y	y	y	8.0E-18	5.0E-14
+ C_2H_3	y	y	y	y	y	y	1.8E-22	1.0E-15
+ C_2H_5	y	y	y	y	y	y	9.8E-25	1.8E-16
+ Cl	n[d]							
+ HS	y	y	y	y	y	y	1.4E-28	3.2E-17
+ NH_2	y	y	y	y	y	y	2.7E-33	8.1E-19
+ O_2	Unst.							

[a] The acronyms have the same meanings as in Table 1, i.e.; TS (y/n), the transition state was/was not found; HR, the hindered rotor scan was/was not successful; HL, high level calculations were/were not successful; S, the correct global symmetry factor was/was not found; W, wells and reactant vdW wells were/were not found; V, variational calculations were/were not successful; Unst denotes that the product is either a very shallow minimum or it is not a well on the PES.
[b] The bold atom denotes the site of the addition.
[c] Rate constants calculated for the 2TS model are reported in cm^3 $molecule^{-1}$ s^{-1} at 300 and 1000 K and compared with a selection of experimental data (in parentheses). This comparison is meant to be representative of reasonably established values, rather than exhaustive.
[d] This reaction may be barrierless.
[e] The product well energy is similar to that of the TS, so that a proper phenomenological rate constant does not exist.
[r] Refers to the reactant side of the PES.

The results reported in Table 3 are again promising. TSs were found for 96% of the reactions, global symmetry factors were always determined correctly and geometries of vdW wells on the reactant side were always found. In one case the TS could not be found and in one case the high level CCSD(T) calculations did not converge at the ROHF stage. The HR algorithms seem to be less resilient than they were for the abstractions; in three cases (10%) the HR optimization strategy had to be modified to obtain meaningful results. This suggests that, in order to use EStokTP reliably for automated studies of addition reactions, it would be necessary to implement post processing algorithms that check the success of EStokTP modules, such as the HR module in this case, and restart the calculations modifying the original options in case of failure. While some of this machinery is already implemented in the current set of algorithms, further work is needed when dealing with HRs for addition reactions.

The results for the ADD42 set are of lower quality. This was expected as this test set, for the same reason explained above for the HAB91 test set, is more challenging than the ADD30 test set. TS

geometries were found only for 89% of the reactions. It seems likely that these failures were largely due to the absence of an energy barrier, and not by an inherent problem with the TS search protocol. Also in this case, although global symmetry factors were always successfully determined, vdW reactant wells were found in only 95% of the cases. In two cases the high level calculations for the TS failed at the RHF step, which prevented the evaluation of a rate constant. IRC calculations were successfully completed for both the ADD30 and ADD42 test sets.

Finally, it can be observed that the mean unsigned error of the common logarithms of the rate constants in their high pressure limit at 300 K is 0.2, while not enough experimental data is available at 1000 K to draw a statistically meaningful conclusion. As found for abstraction reactions, the agreement is again quite good. It should however be mentioned, as highlighted in section 2.10, that when considering larger molecules with several coupled torsional degrees of freedom or when rate constant predictions are determined at lower pressures uncertainties can be expected to increase significantly.

3.4 Isomerization

The most complete protocol for isomerization reactions is very similar to the one shown in Fig. 8c for abstraction. The only difference is that there are no vdW wells present in isomerization reactions. Although we have not prepared an extensive test set for this case, our experience is that it is generally successful, especially for radicals. For closed shell species, difficulties sometimes arise due to the common presence of extensive multireference character in the TS for closed shell isomerizations. In particular, such reactions generally proceed through open shell singlet states (i.e., carbenes), which are well known to require multireference descriptions.

For example, finding the TS for the isomerization of benzene oxide to 2,4 cyclohexadienone was somewhat challenging. At a relatively low level of theory it is possible to determine the TS for this

process by performing the calculations at the spin-unrestricted level and using a broken symmetry guess wave function. The TS can then be found with the isomerization algorithm by performing a grid scan that increases the length of one of the C-O bonds from 1.42 Å to 2.4 Å. The TS structure is shown next to the reactant and product structures in Fig. 14. However, if the grid scan is instead performed on the reacting H, or if a spin-restricted wavefunction is used, the algorithm fails to find a guess structure of sufficient quality for the TS optimization procedure to converge. Thus, an effective EStokTP protocol for arbitrary closed shell isomerizations may require a careful selection of the scanned bond lengths, of the range of the grid scan, as well as of the number of points selected for each scan.

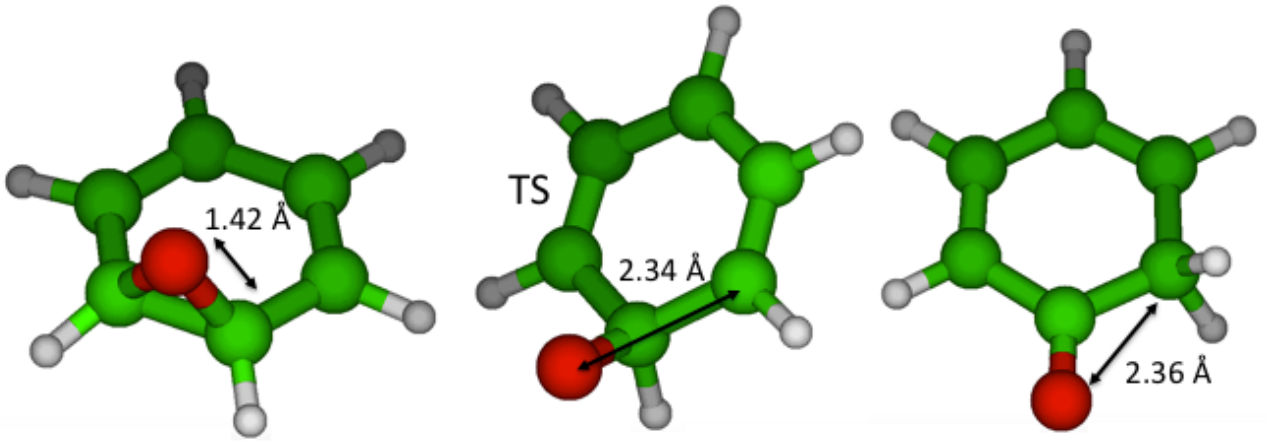

Figure 14. Structures of reactant, product, and TS for the isomerization of benzene oxide to 2,4 cyclohexadienone.

3.5 Beta-scission

Beta-scission reactions are, of course, just the reverse of addition reactions. Thus, the beta-scission protocol is in many ways redundant with the corresponding protocol for addition reactions. Its usefulness lies mostly in the possibility for exploiting this protocol in systematically investigating all possible reaction channels for a given radical. Thus, it will be useful in the construction of PESs performed sequentially by reaction classes through a study of the reactive properties of each well

deemed relevant on the specific portion of the PES that is investigated. The protocols, success ratios, and accuracy are expected to be the same as those reported above for addition reactions.

3.6 Barrierless reactions

Currently, for barrierless reactions, the EStokTP modules can be used to implement variational TST with RRHO approximations corrected by 1D and/or multi dimensional HR treatments, as sketched in Fig. 15. The protocol is organized in three phases. In the first phase, the PES is scanned along the length of the breaking bond (R_{TS}) at theory level 0, which can be for example DFT, until the distance Dist0 is reached. In the second phase, a scan in R_{TS} is initiated at Dist0 for a given interval (e.g., 2 to 4 Å) at a given step (usually 0.1-0.2 Å), with this scan providing the data for the variational determination of the rate constant.

This second scan is performed at theory level 1, which can be specified as a spin-unrestricted wavefunction in DFT or in a single reference post Hartree-Fock method. However, as is well known, for radical-radical reactions such unrestricted single-reference based approaches are plagued by spin contamination and generally lead to significant errors in the PES energy profiles (e.g., typically by several kcal/mol in the key TS region of separations even for CCSD(T)/CBS evaluations). Alternatively, and more properly, this scan should be performed with a multireference method, preferably corrected for dynamic correlation. We have found that CASPT2 is particularly effective for such calculations.

For each optimized point in this second scan Hessian, hindered rotor potentials, and high level energies are determined. These calculations for each grid point are performed in separate EStokTP directories cloned from the directory used in phase 1. Finally, in the third phase the ME blocks produced in the second scan are assembled and a VTST calculation is performed.

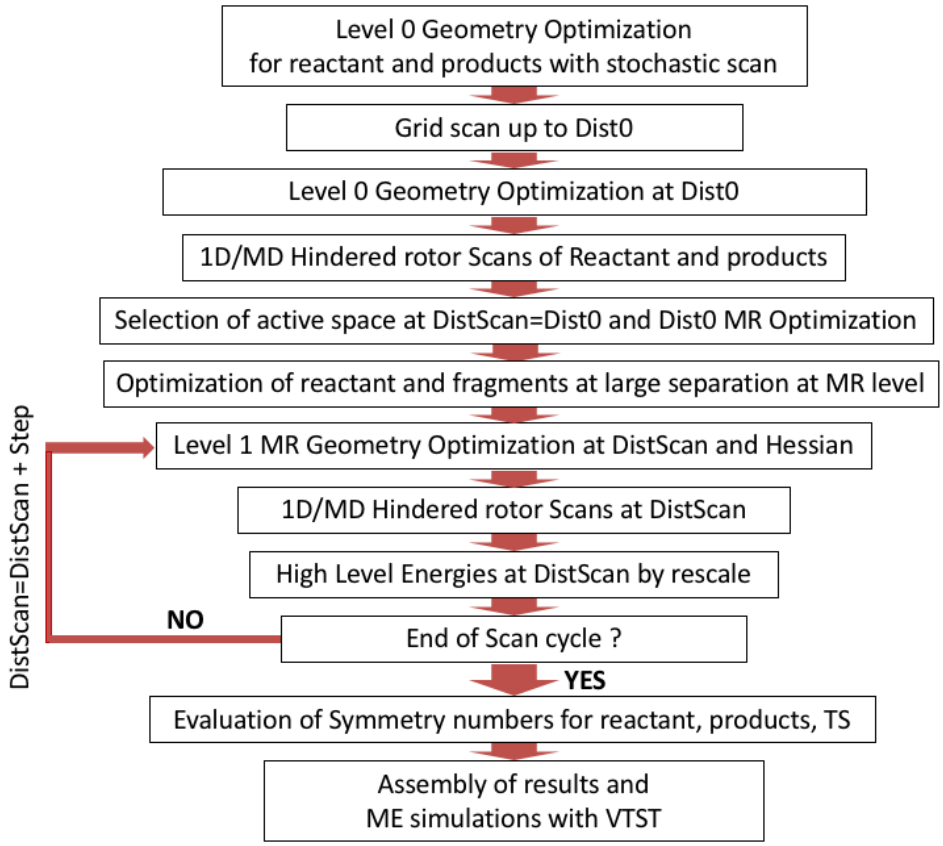

Figure 15. A preliminary protocol for the estimation of rate constants for barrierless reactions. *Dist0* represents the lower edge for a scan over R_{TS} (the length of the breaking bond) with a given number of steps and a stepsize of *Step*. The PES and Hessian along R_{TS} are determined with a suitable multireference (MR) electronic structure method, such as CASPT2.

Automated implementation of this approach for a large set of reactions is still somewhat challenging. First, the implementation of the CASPT2 method requires some specification by the user of the orbital active space, and the best active space to use can often be difficult to determine a priori. A possible solution to this problem is to predetermine a set of optimal active spaces according to the type of bond being broken. Secondly, at large bond separations the scan of the PES can lead to undesirable reorientations of the two reacting moieties. An example of this issue is given below for the decomposition of methanol ($CH_3OH = OH + CH_3$).

It should perhaps also be noted that, for this methodology, limitations in the description of the transitional modes may limit the accuracy of its predictions. In particular, the large amplitude nature of the transitional mode motions may result in significant deviations from the predictions of any reaction path based approach. The variable reaction coordinate TST (VRC-TST) approach[24,129,130] provides a more accurate description of the transitional mode contributions, and we plan to implement a protocol to include this approach within EStokTP in the near future.

To test the accuracy and limitations of the present approach, high pressure rate constants were computed for two reactions for which high quality theoretical and experimental data are available in the literature: the recombination of two methyl radicals to form ethane and the recombination of methyl and OH to form methanol. The first reaction provides a system for which the protocol shown in Fig. 15 should work well, mostly because it is straightforward to define a reliable minimal active space, while the methanol case is expected to be more challenging. For both reactions the calculations were performed at the CASPT2 level; with a (2e,2o) active space for ethane, and a (4e,3o) active space averaged over two states of equal weight for CH_3OH. Calculations were performed using the cc-pVTZ and aug-cc-pVTZ basis sets.

The present predictions for the high pressure recombination rate constants are compared with VRC-TST and other literature results in Fig. 16. This comparison shows that for the recombination of methyl radicals, good agreement can be achieved by using a large basis set and CASPT2 theory, while reasonably satisfactory agreement can be reached for the CH_3 + OH reaction. However, it should be noted that for the CH_3 recombination rate, simulations performed using DFT at the M06-2X/cc-pVTZ level considerably underestimate the rate constant. This failure can be ascribed to the inappropriateness of a single reference method to describe the transition state region of barrierless radical-radical reactions. Meanwhile, for the CH_3 + OH reaction, convergence problems at large separations precluded us from obtaining DFT based rate predictions.

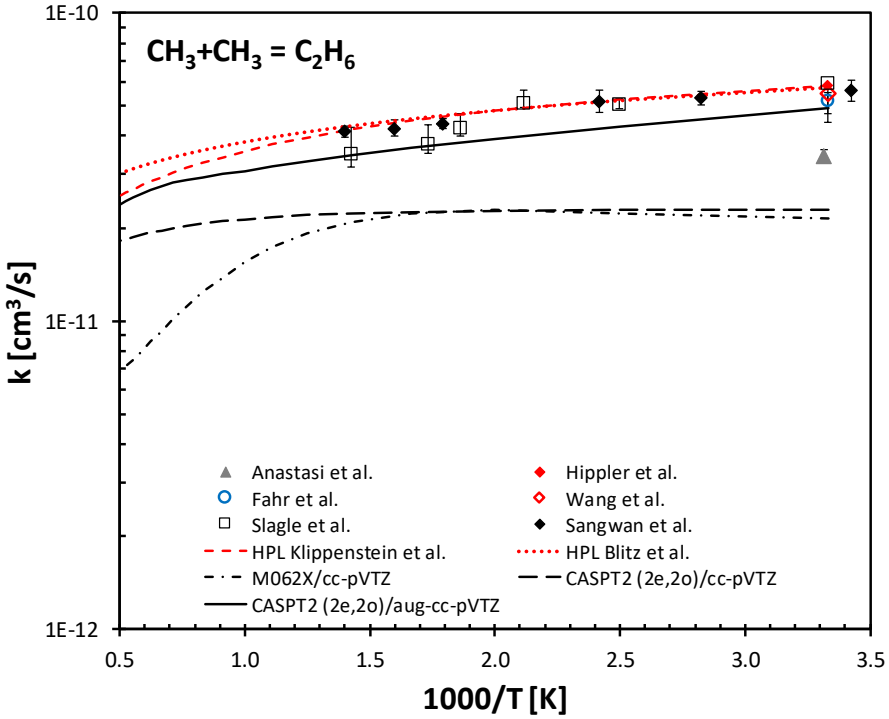

a)

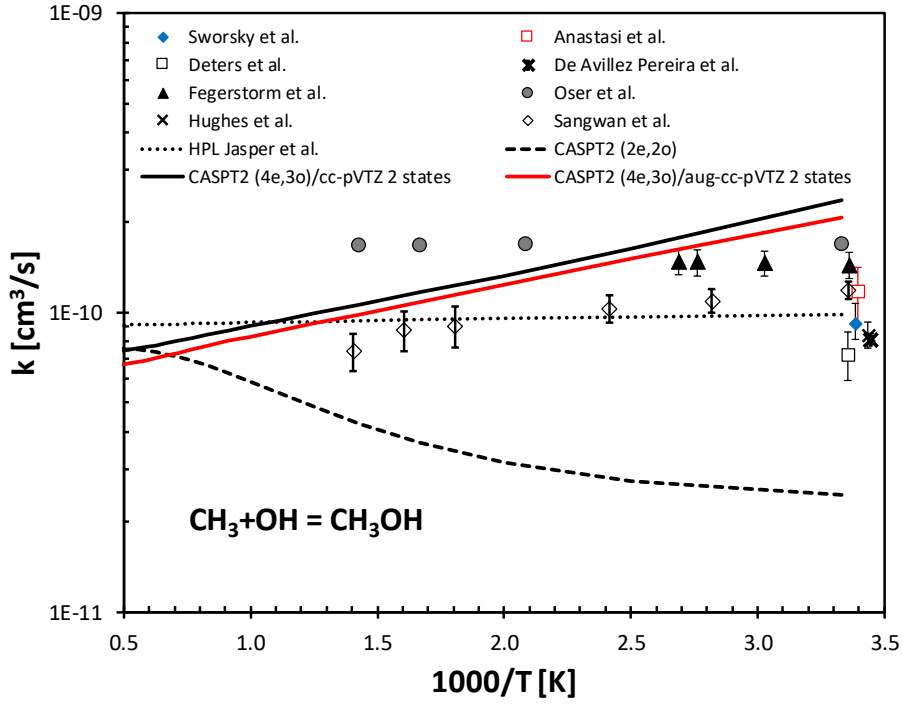

b)

Figure 16. Comparison between the high pressure rate recombination constants calculated with the EStokTP protocol shown in Fig. 15 and VRC-TST and other literature rate constants[129,131-139] for: a) the $CH_3 + CH_3$ recombination reaction and b) the $CH_3 + OH$ recombination reaction.

The simulations for the CH_3 + OH recombination reaction are indicative of the type of challenges that can be expected in automating the rate constant evaluation process for barrierless reactions. First, the sensitivity to the choice of the active space should be noted. The hydroxyl radical has two degenerate electronic states that are only slightly split by spin-orbit interactions and further by interactions with the methyl radical. As a result, a two state multireference wave function that includes both the O lone pair and radical orbital in the active space is required in order to obtain converged wavefunctions throughout the transition state region. These sorts of requirements are an important aspect of any automated active space selection. Secondly, the bond length constrained minimum energy structure changes dramatically as the C-O distance is increased to 3.6 Å and beyond. At these separations, the hydrogen atom of the hydroxyl group is interposed between the C and O atoms forming a H-bond with the C. As a result, the inertia moment of the CH_3-OH 1D-rotor tends to 0, which leads to the failure of the adopted model for internal motions. Notably, this would not be a problem for VRC-TST.

It can thus be reasonably concluded that the proposed EStokTP algorithm for barrierless reactions is promising, but that some challenges still need to be overcome. This will properly require a systematic study similar to the ones performed for abstraction and addition reactions. Notably, the automation of a barrierless reaction algorithm would pave the way for the implementation of VRC-TST theory in EStokTP, which utilizes a high level estimation of the minimum energy path (MEP) energy, and thus to the possibility for estimating highly accurate rate constants for barrierless reactions within the EStokTP framework.

3.7 Multiple Wells reactions

Although EStokTP has been built to determine rate constants of selected classes of single well elementary reactions, it can be readily be used to investigate the kinetics of more complex multi-well multi-channel reactions by exploiting the ME blocks produced from different EStokTP calculations. As explained above, each ME block refers to a single stationary point of a PES, i.e., a

well, or a saddle point, or a grid point in a variational TS analysis. Once generated, these blocks can easily be assembled to generate the input for a multi-well master equation simulation with the MESS solver. The only information that needs to be provided by the user is which wells are connected by each TS included in the PES.

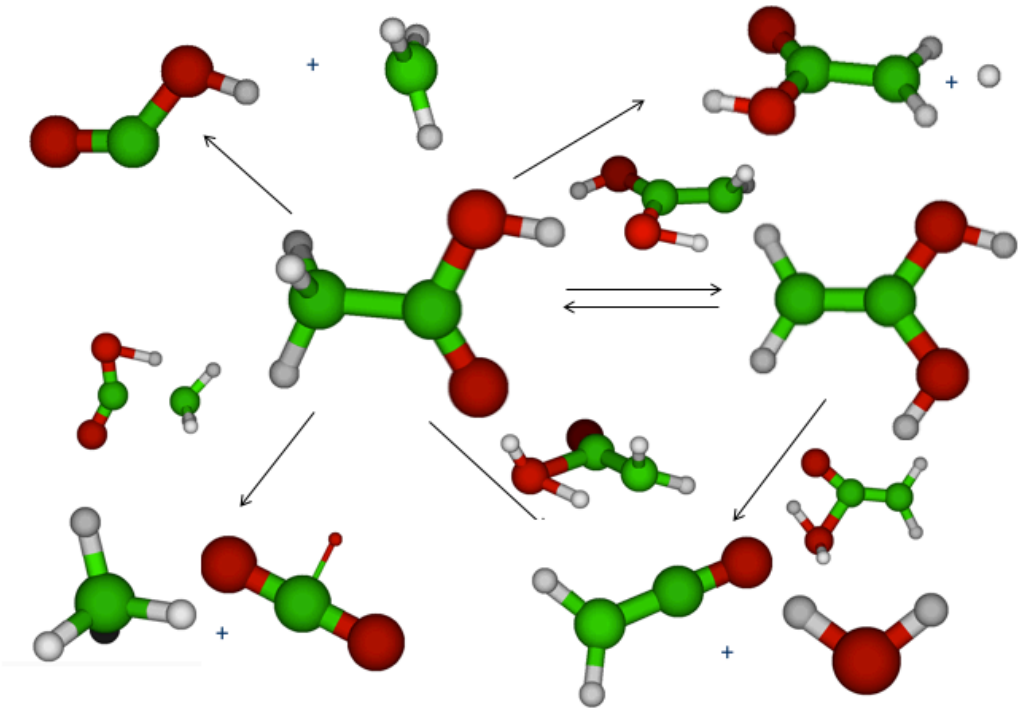

Figure 17. The reaction channels explored in the use of EStokTP to investigate the kinetics of decomposition of acetic acid. [111]

This approach has been used for example to study the kinetics of acetic acid decomposition.[111] The investigated channels are shown in Fig. 17. The rate constants for each individual pathway were investigated through separate EStokTP calculations. Thus, the isomerization of $CH_3C(O)OH$ to CH_2COHOH was studied with the EStokTP isomerization module, the elimination reactions $CH_3C(O)OH \rightarrow CH_2CO + H_2O$, $CH_3COOH \rightarrow CH_4 + CO_2$, and $CH_2COHOH \rightarrow CH_2CO + H_2O$ were studied with the beta-scission module, and the barrierless decompositions $CH_3C(O)OH \rightarrow CH_3 + COOH$ and $CH_3C(O)OH \rightarrow CH_3C(O)O + H$ were investigated using the EStokTP protocol of Fig. 15 for barrierless reactions. The ME simulations yield channel specific rate constants for all the decomposition and isomerization channels, as well as for all the reverse processes. These

simulations required at least one order of magnitude less human time than would have been necessary if the calculations were performed without the assistance of the automated EStokTP protocols.

4. Conclusions and Perspectives

Theoretical chemical kinetics has progressed rapidly in recent years. Nowadays, it is possible to determine rate constants of gas phase reactions at a level of accuracy that is approaching that of experiments. At present the systematic determination of accurate rate constants for large sets of reaction families of kinetic mechanisms is primarily limited by the need for human intervention in the calculations. EStokTP is a computer program that was built to address this issue. In particular, it aims to allow for the determination of the rate constants both automatically and with a high level of accuracy.

In this work we demonstrated that EStokTP is able to automatically determine the rate constants for four classes of reactions: abstraction, addition, isomerization, and beta-scission. Tests performed on a set of about 150 abstraction and 70 addition reactions showed that EStokTP is able to proceed automatically up to the end of the rate constant estimation protocol in more than 90% of cases. A protocol for barrierless reactions, not yet fully automated, has also been developed and shows promising preliminary results. EStokTP can be downloaded from the internet[37] or obtained upon request from the authors.

EStokTP is an ongoing project and is expected to grow significantly in capabilities in the coming years. Several studies are in progress where EStokTP is extensively used. These include the creation of a set of codes to automatically determine the thermodynamic parameters for a list of chemical species starting from a list of structures in SMILES or InChI format[41] and a systematic study of the accuracy of different approaches for the determination of rate constants of abstraction reactions.

ACKNOWLEDGMENTS

Dr. Matteo Pelucchi acknowledges the support of Argonne National Laboratory's visiting graduate program. Prof. Carlo Cavallotti acknowledges the support of the Chemical Sciences and Engineering Division of Argonne National Laboratory for the sabbatical period spent there, during which the main ideas upon which EStokTP is based were developed. The research at ANL was supported in part by the Exascale Computing Project (ECP), Project Number: 17-SC-20-SC, a collaborative effort of two DOE organizations, the Office of Science and the National Nuclear Security Administration, responsible for the planning and preparation of a capable exascale ecosystem including software, applications, hardware, advanced system engineering, and early test bed platforms to support the nation's exascale computing imperative. This material is based on work at ANL supported by the U.S. Department of Energy, Office of Science, Office of Basic Energy Sciences, Division of Chemical Sciences, Geosciences, and Biosciences at Argonne under Contract No. DE-AC02-06CH11357.

Supplementary Information (SI) Available. Description of the ME Block format. This material is available free of charge via the Internet at http://pubs.acs.org.

References

1 Klippenstein, S. J. From Theoretical Reaction Dynamics to Chemical Modeling of Combustion, *Proc. Combust. Inst*. **2017**, *36*, 77-111.

2 Pelucchi, M.; Cavallotti, C.; Faravelli, T.; Klippenstein, S. J. H-Abstraction Reactions by OH, HO_2, O, O_2 and Benzyl Radical Addition to O_2 and Their Implications for Kinetic Modelling of Toluene Oxidation. *Phys. Chem. Chem. Phys*. **2018**, *20*, 10607-10627.

3 Long, A. E.; Merchant, S. S.; Vandeputte, A. G.; Carstensen, H.-H.; Vervust, A. J.; Marin, G. B.; Van Geem, K. M.; Green W. H. Pressure Dependent Kinetic Analysis of Pathways to Naphthalene from Cyclopentadienyl Recombination. *Combust. Flame* **2018**, *187*, 247-256.

4 Wang, K.; Villano, S. M.; Dean, A. M. Ab Initio Study of the Influence of Resonance Stabilization on Intramolecular Ring Closure Reactions of Hydrocarbon Radicals. *Phys. Chem. Chem. Phys.*, **2016**, *18*, 8437-8452.

5 Ye, L.; Xing, L.; Yuan, W.; Li, Y.; Zhang, L.; Qi, F. Predictive Kinetics on the Formation and Decomposition of Ethylbenzene, *Proc. Combust. Inst.* **2017**, *36,* 533-542.

6 Huang, C.; Yang, B.; Zhang, F. Pressure-Dependent Kinetics on the C_4H_7 Potential Energy Surface and its Effect on Combustion Model Predictions. *Combust. Flame* **2017**, *181*, 100-109.

7 Miyoshi, A. Computational Studies on the Reactions of 3-Butenyl and 3-Butenylperoxy Radicals. *Int. J. Chem. Kin.* **2010**, *42*, 273-288

[8] Mebel, A. M.; Georgievskii, Y.; Jasper, A. W.; Klippenstein S. J. Temperature and Pressure-Dependent Rate Coefficients for the HACA Pathways from Benzene to Naphthalene. Proc. Combust. Inst. **2017**, *36*, 919-926.

[9] Li, X.; Jasper, A. W.; Zádor, J.; Miller, J. A.; Klippenstein, S. J. Theoretical Kinetics of O + C_2H_4. Proc. Combust. Inst. **2017,** *36,* 219-227.

[10] Leonori, F.; Balucani, N.; Nevrly, V.; Bergeat, A.; Falcinelli, S.; Vanuzzo, G.; Casavecchia, P.; Cavallotti, C. Experimental and Theoretical Studies on the Dynamics of the O(^{3}P) + Propene Reaction: Primary Products, Branching Ratios and the Role of Intersystem Crossing. *J. Phys Chem. C* **2015**, *119,* 14632-14652.

[11] Wang, H.; You, X.; Blitz, M. A.; Pilling, M. J.; Robertson, S. H. Obtaining Effective Rate Coefficients to Describe the Decomposition Kinetics of the Corannulene Oxyradical at High Temperatures. *Phys. Chem. Chem. Phys.* **2017**, *19*, 11064-11074.

[12] Ali, M. A.; Barker, J. R. Comparison of Three Isoelectronic Multiple-Well Reaction Systems: OH + CH_2O, OH + CH_2CH_2, and OH + CH_2NH. *J. Phys. Chem. A* **2015**, *119*, 7578−7592.

[13] Burke, M. P.; Klippenstein, S. J. Ephemeral Collision Complexes Mediate Chemically Termolecular Transformations that Affect System Chemistry. *Nature Chem*. **2017**, *9*, 1078-1082.

[14] Chen, X.; Goldsmith, C. F. A Theoretical and Computational Analysis of the Methyl-Vinyl + O Reaction and Its Effects on Propene Combustion. *J. Phys. Chem. A* **2017**, *121*, 9173−9184.

[15] Dontgen, M.; Leonhard, K. Discussion of the Separation of Chemical and Relaxational Kinetics of Chemically Activated Intermediates in Master Equation Simulations. *J. Phys. Chem. A* **2017**, *121*, 1563−1570.

[16] Co-optima. http://www.energy.gov/eere/bioenergy/co-optimization-fuels-and-engines. (Accessed November 12, 2018).

[17] Tailored made fules from biomass. http://www.fuelcenter.rwth-aachen.de/. (Accessed November 12, 2018).

[18] Gao, C. W.; Allen, J. W.; Green, W. H.; West, R. H. Reaction Mechanism Generator: Automatic Construction of Chemical Kinetic Mechanisms. *Comp. Phys. Commun*. **2016**, *203*, 212–225.

[19] RMG. https://github.com/ReactionMechanismGenerator/RMG-Py. (Accessed November 12, 2018).

[20] Zheng, J.; Bao, J. L.; Meana-Paneda, R.; Zhang, S.; Lynch, B. J.; Corchado, J. C.; Chuang, Y.-Y.; Fast, P. L.; Hu, W.-P.; Liu, Y.-P.; Lynch, G. C.; Nguyen, K. A.; Jackels, C. F.; Ramos, A. F.; Ellingson, B. A.; Melissas, V. S.; Villa, J.; Rossi, I.; Coitino, E. L.; Pu. J.; Albu, T. V.; Ratkiewicz, A.; Steckler, R.; Garrett, B. C.; Isaacson, A. D.; Truhlar, D. G.; Polyrate 17-C: Computer Program for the Calculations of Chemical Reaction Rates for Polytatomics. University of Minnesota, Minneapolis, MN, 2017; https://comp.chem.umn.edu/polyrate/. (Accessed November 12, 2018).

[21] Zheng, J.; Mielke, S. L.; Bao, J. L.; Meana-Paneda, R.; Clarkson, K. L.; Truhlar, D. G. MSTor: A Program for Calculating Partition Functions, Free Energies, Enthalpies, Entropies, and Heat Capacities of Complex Molecules Including Torsional Anharmonicity. University of Minnesota, Minneapolis, MN, 2017; https://comp.chem.umn.edu/mstor/. (Accessed November 12, 2018).

[22] Zheng, J.; Bao, J. L.; Zhang, S.; Corchado, J. C.; Meana-Pañeda, R.; Chuang, Y.-Y. Coitiño, E. L.; Ellingson, B. A.; Truhlar, D. G. Gaussrate 17-B. https://t1.chem.umn.edu/gaussrate/. (Accessed November 12, 2018).

[23] Georgievskii, Y.; Harding, L. B.; Klippenstein, S. J. VaReCoF. http://tcg.cse.anl.gov/papr/codes/varecof.html. (Accessed November 12, 2018).

[24] Harding, L. B.; Georgievskii, ; Y. Klippenstein, S. J. Predictive Theory for Hydrogen Atom - Hydrocarbon Radical Association Kinetics. *J. Phys. Chem. A*, **2005**, *109*, 4646-4656.

[25] Georgievskii, Y.; Klippenstein, S. J. MESS. http://tcg.cse.anl.gov/papr/codes/mess.html. (Accessed November 12, 2018).

[26] Georgievskii, Y.; Miller, J. A.; Burke, M. P.; Klippenstein, S. J. Reformulation and Solution of the Master Equation for Multiple-Well Chemical Reactions, *J. Phys. Chem. A*, **2013**, *117*, 12146-12154.

[27] Jasper, A. W. NST. http://tcg.cse.anl.gov/papr/codes/nst.html. (Accessed November 12, 2018).

[28] Jasper, A. W. Multidimensional Effects in Nonadiabatic Statistical Theories of Spin-Forbiddenn Kinetics: A Case Study of $^3O + CO \rightarrow CO_2$. *J. Phys. Chem. A* **2015**, *119*, 7339-7351.

[29] Barker, J. R. Multiple-Well, Mulitple-Path Unimolecular Reaction Systems. I. MultiWell Computer Program Suite. *Int. J. Chem. Kinet.* **2001**, *33*, 232-245.

[30] Barker, J. R.; Nguyen, T. L.; Stanton, J. F.; Aieta, C.; Ceotto, M.; Gabas, F.; Kumar, T. J. D.; Li, C. G. L.; Lohr, L. L.; Maranzana, A.; Ortiz, N. F.; Preses, J. M.; Sonk, J. A.; Stimac, P. J. Mutiwell-2017 Software Suite; Barker, J. R. University of Michigan, Ann Arbor, Michigan, USA. http://clasp-research.engin.umich.edu/multiwell/

[31] Glowacki, D. R.; Liang, C. H.; Morley, C.; Pilling, M. J.; Robertson, S. H. MESMER: An Open-Source Master Equation Solver for Multi-Energy Well Reactions. *J. Phys. Chem. A* **2012**, *116*, 9545-9560.

[32] https://www.chem.leeds.ac.uk/mesmer.html and https://sourceforge.net/projects/mesmer/

[33] Bhoorasingh, P. L.; Slakman, B. L.; Khanshan, F. S.; Cain, J. Y.; West, R. H. Automated Transition State Theory Calculations for High-Throughput Kinetics. *J. Phys. Chem. A,* **2017**, *121*, 6896−6904.

[34] Frisch, M. J.; Trucks, G. W.; Schlegel, H. B.; Scuseria, G. E.; Robb, M. A.; Cheeseman, J. R.; Scalmani, G.; Barone, V.; Mennucci, B.; Petersson, G. A. et al. Gaussian 09, Revision A.02; Gaussian, Inc.: Wallingford, CT, 2009.

[35] Allen, J. W.; Green, W. H. CanTherm: Open-Source Software for Thermodynamics and Kinetics. Included in: Reaction Mechanism Generator, v2.0.0., 2016; http://reactionmechanismgenerator.github.io. (Accessed November 12, 2018).

[36] Landrum, G. RDKit: Open-Source Cheminformatics; http://rdkit.org. (Accessed November 12, 2018).

[37] Cavallotti, C.; Pellucchi, M.; Klippenstein, S. J. EStokTP, Electronic Structure to k(T,P); A Program to Generate Rate Constants Relying on Calls to External Codes to Perform Electronic Structure Calculations and Master Equation Simulations. https://github.com/PACChem/EStokTP. (Accessed November 12, 2018).

[38] Eckart, C. The Penetration of a Potential Barrier by Electrons. *Phys. Rev.* **1930**, *35*, 1303−1309.

[39] Liu, Y.-P; Lynch, G. C.; Truong, T. N.; Lu, D. H.; Truhlar, D. G.; Garrett, B. C. Molecular Modeling of the Kinetic Isotope Effect for the [1,5]-Sigmatropic Rearrangement of cis-1,3-Pentadiene. *J. Am. Chem. Soc.* **1993**, *115*, 2408-2415.

[40] Georgievskii, Y.; Klippenstein, S. J. x2z, A Code for Converting from Cartesians to Internals with Well-Defined Torsional Coordinates. https://github.com/PACChem/x2z. (Accessed November 12, 2018).

[41] Keceli, M.; Elliott, S. N.; Li, Y.-P.; Johnson, M. S.; Cavallotti, C.; Georgievskii, Y.; Green, W. H.; Pelucchi, M.; Wozniak, J. M.; Jasper, A. W.; Klippenstein, S. J. Automated Computational Thermochemistry for Butane Oxidation: A Prelude to Predictive Automated Combustion Kinetics. *Proc. Comb. Inst.* **2018**, *37*. https://doi.org/10.1016/j.proci.2018.07.113.

[42] Ahmed, A.; Pitz, W. J.; Cavallotti, C.; Mehl, M.; Lokachari, N.; Nilsson, E. J. K.; Wang, J.-Y.; Konnov, A. A.; Wagnon, S. W.; Chen, B.; Wang, Z.; Kim, S.; Curran, H. J.; Klippenstein, S. J.; Roberts, W. L.; Sarathy, S. M. Small Ester Combustion Chemistry: Computational Kinetics and Experimental Study of Methyl Acetate and Ethyl Acetate. *Proc. Combust. Inst.* **2018**, *37*. https://doi.org/10.1016/j.proci.2018.06.178.

[43] Chai, J. D.; Head-Gordon, M. Systematic Optimization of Long-Range Corrected Hybrid Density Functionals. *J. Chem. Phys.* **2008**, *128*, 084106

[44] Hehre, W. J.; Radom, L.; Pople J. A.; Schleyer, P. v. R. *Ab Initio Molecular Orbital Theory,* Wiley, New York, 1987.

[45] Grimme, S. Semiempirical Hybrid Density Functional with Perturbative Second Order Correlation. *J. Chem. Phys*. **2006,** 124, 034108.

[46] Grimme, S.; Antony, J.; Ehrlich, S.; Krieg, H. A Consistent and Accurate Ab Initio Parameterization of Density Functional Dispersion Correction (DFT-D) for the 94 Elements H-Pu. *J. Chem. Phys.* **2010,** *132*, 154104.

[47] Kendall, R. A.; Dunning, T. H.; Harrison, R. J. Electron Affinities of the First-Row Atoms Revisited. Systematic Basis Sets and Wave Functions. *J. Chem. Phys.* **1992,** *96*, 6796-6806.

[48] Ma, X.; Yang, N.; Johnson, M. A.; Hase, W. L. Anharmonic Densities of States for Vibrationally Excited I–(H_2O), (H_2O)$_2$, and I–(H_2O)$_2$. *J. Chem. Theory Comput.* **2018**, *14*, 3986-3997.

[49] Zheng, J.; Meana-Pañeda, R.; Truhlar, D.G. Prediction of Experimentally Unavailable Product Branching Ratios for Biofuel Combustion: The Role of Anharmonicity. *J. Am. Chem. Soc.* **2014**, *136*, 5150-5160.

[50] Barone, V. Anharmonic Vibrational Properties by a Fully Automated Second-Order Perturbative Approach. *J. Chem. Phys.* **2005**, *122*, 014108.

[51] Alecu, I.M.; Zheng, J.; Zhao, Y.; Truhlar, D. G. Computational Thermochemistry: Scale Factor Databases and Scale Factors for Vibrational Frequencies Obtained from Electronic Model Chemistries. *J. Chem. Theory Comput*. **2010**, *6*, 2872-2887.

[52] Sharma, S.; Raman, S.; Green, W. H. Intramolecular Hydrogen Migration in Alkylperoxy and Hydroperoxyalkylperoxy Radicals: Accurate Treatment of Hindered Rotors. *J. Phys. Chem. A*, **2010,** *114*, 5689-5701.

[53] Zhao, Y.; Truhlar, D. G. The M06 Suite of Density Functionals for Main Group Thermochemistry, Thermochemical Kinetics, Noncovalent Interactions, Excited States, and Transition Elements: Two New Functionals and Systematic Testing of Four M06-Class Functionals and 12 other Functionals. *Theo. Chem. Acc.* **2008**, *120*, 215-241.

[54] Pollak, E.; Pechukas, P. Symmetry Numbers, Not Statistical Factors, Should be used in Absolute Rate Theory and in Bronsted Relations, *J. Am. Chem. Soc.* **1978**, *100*, 2984-2991.

[55] Fernández-Ramos, A.; Ellingson, B. A.; Meana-Pañeda, R.; Marques, J. M. C.; Truhlar, D. G. Symmetry Numbers and Chemical Reaction Rates. *Theor. Chem. Acc.* **2017**, *118*, 813-826.

[56] Natanson, G. A.; Garrett, B. C.; Truong, T. N.; Joseph, T.; Truhlar, D. G. The Definition of Reaction Coordinates for Reaction-Path Dynamic, *J. Chem. Phys.* **1991**, *94*, 7875-7892.

[57] Jackels, C. F. ; Gu, Z.; Truhlar, D. G. Reaction-Path Potential and Vibrational Frequencies in Terms of Curvilinear Internal Coordinates*, J. Chem. Phys.* **1995**, *102*, 3188-3201.

[58] Miller, W. H.; Handy, N. C.; Adams, J. E. Reaction Path Hamiltonian for Polyatomic Molecules. *J. Chem. Phys*. **1980**, *72*, 99-112.

[59] Pechukas, P.; Light, J. C. On Detailed Balancing and Statistical Theories of Chemical Kinetics. *J. Chem. Phys.* **1965**, *42*, 3281-3291.

[60] Nikitin, E. E. *Teor. Eksp. Khim. Acak. Nauk. Ukr. SSR* **1965**, 1, 135.

[61] Jasper, A. W.; Miller, J. A. Lennard-Jones Parameters for Combustion and Chemical Kinetics Modeling from Full-Dimensional Intermolecular Potentials. *Combust. Flame*, **2014**, *161*, 101-110.

[62] Jasper, A. W.; Oana, C. M.; Miller, J. A. "Third-Body" Collision Efficiencies for Combustion Modeling: Hydrocarbons in Atomic and Diatomic Baths. *Proc. Combust. Inst.* **2015**, *35*, 197-204.

[63] Zimmerman, P.M. Growing String Method with Interpolation and Optimization in Internal Coordinates: Method and Examples. *J. Chem. Phys*. **2013,** *138*, 184102.

[64] Peng, C.; Schlegel, H. B. Combining Synchronous Transit and Quasi-Newton Methods for Finding Transition States. *Israel J. Chem.* **1993,** *33*, 449-454.

[65] Miller, W. H. Importance of Nonseparability in Quantum Mechanical Transition-State Theory. *Acc. Chem. Res.* **1976**, *9*, 306-312.

[66] Sun, L.; Song, K.; Hase, W.L. A S_N2 reaction that Avoids its Deep Potential Energy Minimum. *Science*, **2002**, *296*, 875-878.

[67] Xie, J.; Sun, R.; Siebert, M. R.; Otto, R.; Wester, R.; Hase, W. L. Direct Dynamics Simulations of the Product Channels and Atomistic Mechanisms for the OH- + CH_3I Reaction: Comparison with Experiment. *J. Phys. Chem. A* **2013**, *117*, 7162-7178.

[68] Jasper, A. W.; Pelzer, K. M.; Miller, J. A.; Kamarchik, E.; Harding, L. B.; Klippenstein, S. J. Predictive a priori pressure-dependent kinetics. *Science* **2014**, *346*, 1212-1215.

[69] Keceli, M.; Elliott, S. N.; Klippenstein, S. J. QTC: Python Modules for Quantum Thermochemistry Calculations. https://github.com/keceli/QTC. (Accessed November 12, 2018).

[70] Elliott, S. N.; Keceli, M.; Klippenstein, S. J. TorsScan: Python Modules for Employing EStokTP in the Generation of NASA Polynomial Representations of Thermochemistry. https://github.com/snelliott/TorsScan. (Accessed November 12, 2018).

[71] Lam, K. -Y.; Davidson, D. F.; Hanson, R. K. High-Temperature Measurements of the Reactions of OH with Small Methyl Esters: Methyl Formate, Methyl Acetate, Methyl Propanoate, and Methyl Butanoate *J. Phys. Chem. A* **2012,** *116*, 12229-12241.

[72] El Boudali, A.; Le Calvé, S.; Le Bras, G.; Mellouki, A. Kinetic Studies of OH Reactions with a Series of Acetates. *J. Phys. Chem.* **1996,** *100*, 12364-12368

[73] Smith, D. F.; McIver, C. D.; Kleindienst, T. E. Kinetics and Mechanism of the Atmospheric Oxidation of tertiary amyl methyl ether. *Int. J. Chem. Kinet*. **1995**, *27*, 453 – 472.

[74] Sutherland, J. W.; Su, M.-C.; Michael, J. V., Rate Constants for H + CH_4, CH_3 + H_2, and CH_4 Dissociation at High Temperature. *Int. J. Chem. Kinet*. **2001,** *33*, 669-684.

[75] Srinivasan, N. K.; Su, M. C.; Sutherland, J. W.; Michael, J. V.; Reflected Shock Tube Studies of High-Temperature Rate Constants for OH + $CH_4 \rightarrow CH_3 + H_2O$ and $CH_3 + NO_2 \rightarrow CH_3O + NO$. *J. Phys. Chem. A*, **2005,** 109, 1857-1863.

[76] Baldwin, R. R.; Jones, P. N.; Walker, R. W. Determination of the Rate Constant for HO_2 + CH_4 $\rightarrow$ H_2O_2 + CH_3 at 443°C. *J. Chem. Soc. Faraday Trans*. **1988,** *84*, 199–207.

[77] Miyoshi, A.; Tsuchiya, K.; Yamauchi, N.; Matsui, H., Reactions of Atomic Oxygen (^{3}P) with Selected Alkanes. *J. Phys. Chem*. **1994,** *98*, 11452–11458.

[78] Sivaramakrishnan, R.; Michael, J. V.; Ruscic, B. High-Temperature Rate Constants for H/D + C_2H_6 and C_3H_8. *Int. J. Chem. Kinet*., **2012,** *44*, 194–205.

[79] Krasnoperov, L. N.; Michael, J. V. Shock Tube Studies Using a Novel Multipass Absorption Cell: Rate Constant Results for OH + H_2 and OH + C_2H_6. *J. Phys. Chem. A*, **2004,** *108*, 5643–5648.

[80] Vasu, S. S.; Hong, Z. K.; Davidson, D. F.; Hanson, R. K.; Golden, D. M.; Shock Tube/Laser Absorption Measurements of the Reaction Rates of OH with Ethylene and Propene. *J. Phys. Chem. A*, **2010**, 114, 11529–11537.

[81] Peeters, J.; Van Look, H.; Ceursters, B.. Absolute Rate Coefficients of the Reactions of C_2H with NO and H_2 between 295 and 440 K. *J. Phys. Chem.* **1996,** 100, 15124–15129.

[82] Keil, D. G.; Tanzawa, T.; Skolnik, E. G.; Klemm, R. B.; Michael, J. V. Rate Constants for the Reaction of Ground State Atomic Oxygen with Methanol; *J. Chem. Phys.* **1981,** *75*, 2693-2704.

[83] Sivaramakrishnan, R.; Michael, J. V.; Wagner, A. F.; Dawes, R.; Jasper, A. W.; Harding, L. B.; Georgievskii, Y.; Klippenstein, S. J. Roaming Radicals in the Thermal Decomposition of Dimethyl Ether: Experiment and Theory. *Combust. Flame*, **2011,** *158*, 618-632.

[84] Carr, S. A.; Still, T. J.; Blitz, M. A.; Eskola, A. J.; Pilling, M. J.; Seakins, P. W.; Shannon, R. J.; Wang, B.; Robertson, S. H., Experimental and Theoretical Study of the Kinetics and Mechanism of the Reaction of OH Radicals with Dimethyl Ether, *J. Phys. Chem. A*, **2013**, *117*, 11142-11154.

[85] Cook, R. D.; Davidson, D. F.; Hanson, R. K. High-Temperature Shock Tube Measurements of Dimethyl Ether Decomposition and the Reaction of Dimethyl Ether with OH. *J. Phys. Chem. A*, **2009,** *113*, 9974-9980.

[86] Liu, R.; Dagaut, P.; Huie, R. E.; Kurylo, M. J. A Flash Photolysis Resonance Fluorescence Investigation of the Reactions of Oxygen O(^{3}P) Atoms with Aliphatic Ethers and Eiethers in the Gas Phase. *Int. J. Chem. Kinet*., **1990**, *22*, 711–717.

[87] Takahashi, K.; Yamamoto, O.; Inomata, T.; Kogoma, M. Shock-Tube Studies on the Reactions of Dimethyl Ether with Oxygen and Hydrogen Atoms, *Int. J. Chem. Kinet.* **2007,** *39*, 97–108.

[88] Oehlers, C.; Wagner, H. Gg.; Ziemer, H.; Temps, F.; Dobe, S. An Investigation of the D/H Addition-elimination and H Atom Abstraction Channels in the Reaction D + H_2CO in the Temperature Range 296<=T<=780 K. *J. Phys. Chem. A*, **2000,** *104*, 10500–10510.

[89] Vasudevan, V.; Davidson, D. F.; Hanson, R. K. Atoms Regeneration from Hydroperoxyl Radicals in the Reaction between Fluorine and Hydrogen Inhibited with Oxygen. *Int. J. Chem. Kinet.* **2005**, *37*, 98–109.

[90] Taylor, P. H.; Jiang, Z.; Dellinger, B.; Determination of the Gas-Phase Reactivity of Hydroxyl with Chlorinated Methanes at High Temperature: Effects of Laser/Thermal Photochemistry. *Int. J. Chem. Kinet.;* **1993**, *25*, 9–23.

[91] Ko, T.; Fontijn, A.; Lim, K. P.; Michael, J. V. A Kinetics Study of the $O(^3P)$ + CH_3Cl Reaction Over the 556-1485 K Range by the HTP and LP-ST Techniques *Symp. Int. Combust. Proc.* **1992,** *14*, 735–742.

[92] Yoshimura, M.; Koshi, M.; Matsui, H.; Kamiya, K.; Umeyama, H. Non-Arrhenius Temperature Dependence of the Rate Constant for the H + H_2S Reaction. *Chem. Phys. Lett.* **1992**, *189*; 199-204.

[93] Westenberg, A. A.; DeHaas, N. Rate of the Reaction OH + H_2S → SH + H_2O over an Extended Temperature Range; *J. Chem. Phys.* **1973,** *59*, 6685-6686.

[94] Sutherland, J. W.; Michael, J. V. The kinetics and thermodynamics of the reaction H+ NH_3⇄ NH_2+H_2 by the flash photolysis–shock tube technique: Determination of the equilibrium constant, the rate constant for the back reaction, and the enthalpy of formation of the amidogen radical. *J. Chem. Phys.* **1987,** *88***,** 830-834.

[95] Michael, J. V.; Sutherland, J. W.; Klemm, R. B. Rate Constant for the Reaction H + NH_3 Over the Temperature Range 750-1777 K. *J. Phys. Chem.* **1986**, *90*, 497-500.

[96] Diau, E. W.-G.; Tso, T.-L.; Lee, Y.-P. Kinetics of the Reaction OH + NH_3 in the Range 273-433 K, *J. Phys. Chem.* **1990,** *94*, 5261-5265.

[97] Cohen, N.; Westberg, K. R. Chemical Kinetic Data Sheets for High-Temperature Reactions. Part II. *J. Phys. Chem. Ref. Data* **1991**, *20*, 1211–1311.

[98] Sutherland, J. W.; Patterson, P. M.; Klemm, R. B. Flash Photolysis-Shock Tube Kinetic Investigation of the Reaction of $O(^3P)$ Atoms with Ammonia. *J. Phys. Chem.* **1990**, *94*, 2471-2475.

[99] Ceursters, B.; Nguyen, H. M. T.; Peeters, J.; Nguyen, M. T. Experimental and Theoretical Study of the Gas Phase Reaction of Ethynyl Radical with Methane (HCC + CH_4). *Chem. Phys. Lett.* **2000**, *329*, 412–420.

[100] Bryukov, M. G.; Slagle, I. R.; Knyazev, V. D. Kinetics of Reactions of Cl Atoms with Methane and Chlorinated Methanes, *J. Phys. Chem. A* **2002**, *106*, 10532-10542.

[101] Demissy, M.; Lesclaux, R. Kinetics of Hydrogen Abstraction by NH_2 Radicals from Alkanes in the Gas Phase. A Flash Photolysis-Laser Resonance Absorption Study. *J. Am. Chem. Soc.* **1980**, *102*, 2897-2902.

[102] Hack, W.; Kurzke, H.; Rouveirolles, P.; Wagner, H.Gg. Direct Measurements of the Reaction NH_2 + CH_4 → NH_3 + CH_3 in Temperature Range 743-1023; *Symp. Int. Combust. Proc*. **1986**, *21*, 905-911.

[103] Opansky, B. J.; Leone, S. R. Rate Coefficients of C_2H with C_2H_4, C_2H_6, and H_2 from 150 to 359 K. *J. Phys. Chem.* **1996**, *100*, 19904–19910.

[104] Hickson, K. M.; Bergeat, A.; Costes, M. A Low Temperature Study of the Reactions of Atomic Chlorine with Simple Alkanes. *J. Phys. Chem. A*, **2010**, *114*, 3038-3034.

[105] Bryukov, M. G.; Slagle, I. R.; Knyazev, V. D. Kinetics of Reactions of Cl Atoms with Ethane, Chloroethane, and 1,1-Dichloroethane. *J. Phys. Chem. A,* **2003**, *107*, 6565-6573.

[106] Kaiser, E. W.; Wallington, T. J. Kinetics of the Reactions of Chlorine Atoms with C_2H_4 (k_1) and C_2H_2 (k_2): A Determination of $\Delta Hf,298°$ for C_2H_3. *J. Phys. Chem*. **1996**, 100, 4111–4119.

[107] Seakins, P. W.; Orlando, J. J.; Tyndall, G. S. Rate Coefficients and Production of Vibrationally Excited HCl From the Reactions of Chlorine Atoms with Methanol, Ethanol, Acetaldehyde and Formaldehyde. *Phys. Chem. Chem. Phys*. **2004**, *6*, 2224 – 2229.
[108] Srinivasan, N. K.; Su, M. C.; Sutherland, J. W.; Michael, J. V. Reflected Shock Tube Studies of High-Temperature Rate Constants for $CH_3 + O_2$, $H_2CO + O_2$, and $OH + O_2$, *J. Phys. Chem. A*, **2005**, 109, 7902–7914.
[109] Sarzynski, D.; Gola, A. A.; Drys, A.; Jodkowski, J. T. Kinetic Study of the Reaction of Chlorine Atoms with Chloromethane in the Gas Phase. *Chem. Phys. Lett*. **2009**, 476, 138–142.
[110] Gao, Y. D.; Alecu, I. M.; Hsieh, P. C.; Morgan, B. P.; Marshall, P.; Krasnoperov, L. N.; Thermochemistry is Not a Lower Bound to the Activation Energy of Endothermic Reactions: A Kinetic Study of the Gas-Phase Reaction of Atomic Chlorine with Ammonia. *J. Phys. Chem. A*, **2006**, *110*, 6844–6850.
[111] Cavallotti, C.; Pelucchi, M.; Frassoldati, A. Analysis of Acetic Acid Gas Phase Reactivity: Rate Constant Estimation and Kinetic Simulations. *Proc. Combust. Inst.* **2018**, *37*, 10.1016/j.proci.2018.06.137.
[112] Gilbert, T.; Grebner, T.L.; Fischer, I.; Chen, P. Microcanonical rates for the unimolecular dissociatin of the ethyl radical. *J. Chem. Phys.* **1999**, *110*, 5485-5488.
[113] Hase, W.L.; Schlegel, H.B.; Balbyshev, V.; Page, M. An ab Initio Study of the Transition State and Forward and Reverse Rate Constants for $C_2H_5 \rightleftharpoons H + C_2H_4$. *J. Phys. Chem. A* **1996**, *100*, 5354-5361.
[114] Miller, J. A.; Klippenstein, S. J. The $H + C_2H_2$ (+M) = C_2H_3 (+M) and $H + C_2H_2$ (+M) = C_2H_5 (+M) Reactions: Electronic Structure, Variational Transition State Theory, and Solutions to a Two-Dimensional Master Equation. *Phys. Chem. Chem. Phys.* **2004**, *6*, 1192-1202.
[115] Lightfoot, P. D.; Pilling, M. J. Temperature and Pressure Dependence of the Rate Constant for the Addition of Hydrogen Atoms to Ethylene. *J. Phys. Chem.* **1987**, *91*, 3373-3379.
[116] Lee, J. H.; Michael, J. V.; Payne, W. A.; Stief. L. J. Absolute Rate of the Reaction of Atomic Hydrogen with Ethylene from 198 to 320 K at High Pressure. *J. Chem. Phys.* **1978,** *68*, 1817-1820.
[117] Hanning-Lee, M. A.; Green, N. J. B.; Pilling, M. J. Direct Observation of Equilibration in the System $H + C_2H_4 = C_2H_5$: Standard Enthalpy of Formation of the Ethyl Radical. *J. Phys. Chem.* **1993**, *97*, 860-870.
[118] Sugawara, K.; Okazaki, K.; Sato, S. The Rate Constants of the Reactions of Hydrogen and Oxygen Atoms with Fluoroethylenes. *Bull. Chem. Soc. Japan* **1981,** *54*, 358-361.
[119] Lightfoot, P.D.; Pilling, M.J. Temperature and pressure dependence of the rate constant for the addition of H to C_2H_4. *J. Phys. Chem*. **1987**, *91*, 3373 - 3379.
[120] Cleary, P. A.; Romero, M. T. B.; Blitz, M. A.; Heard, D. E.; Pilling, M. J.; Seakins, P. W.; Wang, L. Determination of the Temperature and Pressure Dependence of the Reaction OH + C_2H_4 from 200-400 K Using Experimental and Master Equation Analyses. *Phys. Chem. Chem. Phys.* **2006**, *8,* 5633–5642.
[121] Knyazev, V. D.; Slagle, I. R. Experimental and Theoretical Study of the $C_2H_3 = H + C_2H_2$ reaction. Tunneling and the Shape of Falloff Curves. *J. Phys. Chem*. **1996,** *100*, 16899–16911.
[122] Mckee, K. W.; Blitz, M. A.; Cleary, P. A.; Glowacki, D. R.; Pilling, M. J.; Seakins, P. W.; Wang, L. M. Experimental and Master Equation Study of the Kinetics of $OH + C_2H_2$: Temperature Dependence of the Limiting High Pressure and Pressure Dependent Rate Coefficients. *J. Phys. Chem. A* **2007**, *111*, 4043–4055.
[123] Sheaffer, P. M.; Zittel, P. F. UV to Near-IR CO Emissions from $O + C_2H_2$ and $O + C_3O_2$ Flames at Low Pressure and High Temperature. *J. Phys. Chem. A* **2000**, *104*, 10194–10201.
[124] Michael, J. V.; Wagner, A. F. Rate Constants for the Reactions $O + C_2H_2$ and $O + C_2D_2 \rightarrow$ Products, Over the Temperature Range ~850-1950 K, by the Flash Photolysis-Shock Tube

Technique. Determination of the Branching Ratio and a Further Theoretical Analysis; *Ber. Bunsenges. Phys. Chem*. **1990**, 94, 2453–2464.

[125] Ismail, H.; Goldsmith, C. F.; Abel, P. R.; Howe, P. T.; Fahr, A.; Halpern, J. B.; Jusinski, L. E.; Georgievskii, Y.; Taatjes, C. A.; Green, W. H. Pressure and Temperature Dependence of the Reaction of Vinyl Radical with Ethylene. *J. Phys. Chem. A* **2007**, *111*, 6843-6851.

[126] Carl, S. A. A Highly Sensitive Method for Time-Resolved Detection of O(^{1}D) Applied to Precise Determination of Absolute O(^{1}D) Reaction Rate Constants and O(^{3}P) Yields. *Phys. Chem. Chem. Phys.* **2005**, *7,* 4051–4053.

[127] Callear, A. B.; Smith, G. B. Addition of Atomic Hydrogen to Acetylene. Chain Reactions of the Vinyl Radical. *Chem. Phys. Lett.* **1984**, *105*, 119-122.

[128] Perner, D.; Franken, Th. Untersuchung von Primarprozessen an Gasformigem Schwefelwasserstoff mit Hilfe der Pulsradiolyse. *Ber. Bunsenges. Phys. Chem*. **1969**, *73*, 897.

[129] Klippenstein, S. J.; Georgievskii, Y.; Harding, L. B. Predictive Theory for the Combination Kinetics of Two Alkyl Radicals. *Phys. Chem. Chem. Phys.* **2006**, *8*, 1133-1147.

[130] Klippenstein, S. J. Variational Optimizations in the Rice-Ramsperger-Kassel-Marcus Theory Calculations for Unimolecular Dissociations with No Reverse Barrier. *J. Chem. Phys.* **1992**, *96*, 367-371.

[131] Sangwan, M.; Yan, C.; Chesnokov, E. N.; Krasnoperov, L. N. Reaction $CH_3 + CH_3 \rightarrow C_2H_6$ Studied over the 292-714 K Temperature and 1-100 bar Pressure Ranges. *J. Phys. Chem. A* **2015**, *119*, 7847-7857.

[132] Blitz, M. A.; Green, N. J. B.; Shannon, R. J.; Pilling, M. J.; Seakins, P. W.; Western, C. M.; Robertson, S. H. Reanalysis of Rate Data for the Reaction $CH_3 + CH_3 \rightarrow C_2H_6$ Using Revised Cross Sections and a Linearized Second-Order Master Equation. *J. Phys. Chem. A* **2015**, *119*, 7668-7682.

[133] Miller, J. A.; Klippenstein, S. J. The $H + C_2H_2$ (+ M) $\rightleftarrows C_2H_3$ (+M) and $H + C_2H_2$ (+M) $\rightleftarrows C_2H_5$ (+M) reactions: Electronic structure, variational transition-state theory, and solutions to a two-dimensional master equation. *Phys. Chem. Chem. Phys.* **2004**, *6*, 1192-1202.

[134] Anastasi, C.; Arthur, N. L. Rate Constants for the Reactions of CH_3 radicals with C_2H_5, iC_3H_7 and tC_4H_9 Radicals. *J. Chem. Soc., Faraday Trans.* 2 **1987**, *83*, 277-287.

[135] Hippler, H.; Luther, K.; Ravishankara, A. R.; Troe, J. High-Pressure Effects in the Recombination Reaction $CH_3 + CH_3 \rightarrow C_2H_6$. *Zeit. Phys. Chem.* **1984**, *142*, 1-12.

[136] Fahr, A.; Laufer, A.; Klein, R.; Braun, W. Reaction Rate Determinations of Vinyl Radical Reactions with Vinyl, Methyl, and Hydrogen Atoms. *J. Phys. Chem.* **1991**, *95*, 3218-3224.

[137] Wang, B.; Hou, H.; Yoder, L. M.; Muckerman, J. T.; Fockenberg, C. Experimental and Theoretical Investigations on the Methyl−Methyl Recombination Reaction. *J. Phys. Chem. A* **2003**, *107*, 11414-11426.

[138] Slagle, I. R.; Gutman, D.; Davies, J. W.; Pilling, M. J. Study of the Recombination Reaction Methyl + Methyl → Ethane. 1. Experiment. *J. Phys. Chem.* **1988**, *92*, 2455-2462.

[139] Sangwan, M.; Yan, C.; Chesnokov, E. N.; Krasnoperov, L. N. Reaction $CH_3 + CH_3 \rightarrow C_2H_6$ Studied over the 292–714 K Temperature and 1–100 Bar Pressure Ranges. *J. Phys. Chem. A* **2015**, *119*, 7847-7857.

Table of Content Graphic

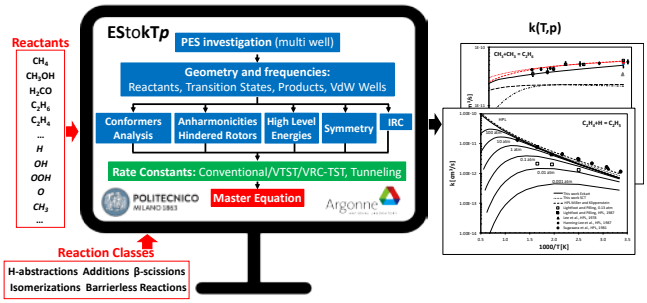

Supporting Information for

EStokTP:

Electronic Structure to Temperature and Pressure Dependent Rate Constants;

A Code for Automatically Predicting the Thermal Kinetics of Reactions

C. Cavallotti[1], M. Pelucchi[1], Y. Georgievskii[2], S. J. Klippenstein[2]

This file contains

S1. The ME Block structure format: the concept

The master equation (ME) block format is a concept that took shape while writing EStokTP and thinking how the portion of the data generated through the electronic structure calculations that are relevant for single channel ME calculations could be organized so that they could subsequently be used to set up the master equation input for a Multiwell and/or multichannel PES. Ultimately, it was realized that such ME blocks are also useful for store information for various other uses, such as for creating a database of reactant and product species.

In the ME block format all the information necessary to run a ME for each stationary point on the PES, be it a well or a saddle point, are stored in a single file, with the associated electronic energy, corrected with ZPE, stored both in the file and in a separate file. The structure of a ME block is consistent with the input structure of the MESS solver, for which a manual is available (http://tcg.cse.anl.gov/papr/codes/mess.html) with detailed description of the meaning of the used keywords. In the following sections we provide descriptions of the ME block format for wells (section S2), bimolecular species (section S3), conventional TS (section S4), and variational TS (section S5).

S2. ME Block structure format: well

The ME block for ethane is reported below. The file contains: xyz geometry, in Angstrom, global symmetry factor (includes optical symmetry number), hindered rotor potential, frequencies (in rows of ten values), energy, and electronic energy levels (in cm^{-1}) with degeneracy. The whole hindered rotor section should be repeated for as many times as there are hindered rotors.

```
!-------------------------------------------------------------------------------------------------
Well REAC1
  Species
  RRHO
    Geometry[angstrom]            8
      C    0.00000   0.00000   0.00000
      C    0.00000   0.00000   1.52350
      H    1.01566   0.00000   1.91771
      H   -0.50781   0.87960   1.91769
       H   -0.50782  -0.87958   1.91770
      H    0.50792  -0.87953  -0.39418
      H   -1.01567  -0.00013  -0.39417
      H    0.50770   0.87966  -0.39417
    Core         RigidRotor
      SymmetryFactor    6.0000000000000000
    End
    Rotor                Hindered
      Group              6   7   8
      Axis               1   2
      Symmetry           3
      Potential[kcal/mol]       12
        0.00    0.17    0.64    1.30    2.00    2.53    2.73    2.53    2.00    1.30    0.64    0.17
    End
    Frequencies[1/cm]          17
      3144.4   3143.6   3121.1   3120.3   3067.8   3066.2   1510.2   1509.9   1508.2   1507.8
      1424.3   1406.1   1222.1   1221.8   1020.2   823.89   822.63
    ZeroEnergy[kcal/mol]      0.
    ElectronicLevels[1/cm]    1
        0.0000000000000000       1.0000000000000000
  End
 End
!***********************************
!-------------------------------------------------------------------------------------------------
```

S3. ME Block structure format: bimolecular species

The ME block structure for reactants or products consisting of two species has a dedicated format, similar to the one used for wells (section S2). The ME bimolecular block for ethane and H is reported below.

```
!-------------------------------------------------------------------------------------------------------
Bimolecular BIMOL1
  Fragment REACT1
  RRHO
    Geometry[angstrom]              8
      C    0.00000   0.00000   0.00000
      C    0.00000   0.00000   1.52350
      H    1.01566   0.00000   1.91771
      H   -0.50781   0.87960   1.91769
      H   -0.50782  -0.87958   1.91770
      H    0.50792  -0.87953  -0.39418
      H   -1.01567  -0.00013  -0.39417
      H    0.50770   0.87966  -0.39417
    Core          RigidRotor
      SymmetryFactor    6.0000000000000000
    End
    Rotor                 Hindered
      Group               6   7   8
      Axis                1   2
      Symmetry                  3
      Potential[kcal/mol]       12
        0.00    0.17    0.64    1.30    2.00    2.53    2.73    2.53    2.00    1.30    0.64    0.17
    End
    Frequencies[1/cm]           17
      3144.4   3143.6   3121.1   3120.3   3067.8   3066.2   1510.2   1509.9   1508.2   1507.8
      1424.3   1406.1   1222.1   1221.8   1020.2   823.89   822.63
    ZeroEnergy[kcal/mol]      0.
    ElectronicLevels[1/cm]    1
      0.0000000000000000       1.0000000000000000
!***********************************
  End
!*********
  Fragment REACT2
  Atom
    Name H
    ElectronicLevels[1/cm]    1
      0.0000000000000000       2.0000000000000000
!***********************************
  End
!*********
  GroundEnergy[kcal/mol] 0.0
End
!-------------------------------------------------------------------------------------------------------
```

S4. ME Block structure format: conventional transition state

The ME block structure for a conventional TS is similar to the one used for the wells. In the following the ME block for the C_2H_6 + H abstraction reaction is reported. The first line means that this is a TS with a barrier that connects the species 'REAC1' and the species 'WR', each of which should be defined by one of the ME block structures described in section S2 (single well) or S3 (bimolecular).
Please note the presence of the tunneling section that, for the Eckart model, requires as information the imaginary frequency and the heights of the forward and backward barriers.

```
!-------------------------------------------------------------------------------------------------
Barrier TS REAC1 WR
  RRHO     ! transition state
    Geometry[angstrom]            9
      C    0.00000   0.00000   0.00000
      C    0.00000   0.00000   1.50264
      H    1.01547   0.00000   1.89712
      H   -0.51559   0.87483   1.89711
      H   -0.50570  -0.88508   1.89624
      H    0.60163  -0.76824  -0.47615
      H   -0.96762   0.12597  -0.47615
      H    0.64545   1.13284  -0.37168
      H    1.09252   1.91810  -0.56192
    Core    RigidRotor
      SymmetryFactor    1.0000000000000000
    End
    Rotor                 Hindered
      Group               6   7   8   9
      Axis                1   2
      Symmetry            3
      Potential[kcal/mol]           4
        0.00    0.89    1.83    0.89
    End
    Frequencies[1/cm]          19
      3197.0   3136.0   3118.3   3108.4   3050.9   1610.2   1493.3    1493.2   1469.0   1404.5
      1234.1   1181.7   1173.8   1114.2   1037.7   863.99   827.46   545.94   294.24
    ZeroEnergy[kcal/mol]               9.77
    ElectronicLevels[1/cm]             1
      0.0000000000000000               2.0000000000000000
    Tunneling    Eckart
      ImaginaryFrequency[1/cm]      1457.0200000000000
      WellDepth[kcal/mol]           9.77
      WellDepth[kcal/mol]           13.81
    End
  End
!***********************************
End
!-------------------------------------------------------------------------------------------------
```

S5. ME Block structure format: variational transition state

The variational TS is in many ways simply a extension of the conventional TS ME block structure shown in section S4. For it, the key RRHO subcomponent is repeated n times, where n is the number of variational grid points. Here we report a sample block structure for C_2H_6 + H. The number of variational structures reported in the input can be as many as desired. For simplicity, only two are reported here.

```
!-------------------------------------------------------------------------------------------------
Barrier B2 WR WP
  Variational
    RRHO          !           Structure 1
      Geometry[angstrom]          9
        C   -0.03959  -0.06950  -0.70733
        C   -0.04483  -0.07870   0.79935
        H    0.97068  -0.07761   1.19347
        H   -0.55961   0.79667   1.19347
        H   -0.55017  -0.96323   1.19122
        H    0.54826  -0.85519  -1.17507
        H   -1.01518   0.03575  -1.17508
        H    0.54978   0.96483  -1.05228
        H    1.06140   1.86348  -1.27132
      Core       RigidRotor
        SymmetryFactor    1.0000000000000000
      End
      Rotor                       Hindered
        Group                     6   7   8   9
        Axis                      1   2
        Symmetry                  3
        Potential[kcal/mol]           4
          0.00    0.89    1.83    0.89
      End
      Frequencies[1/cm]          19
        3181.7   3135.5   3121.0   3103.8    3059.5   1500.6   1500.3    1471.7   1412.2   1351.3
        1339.9   1297.9   1220.6   1187.3   1040.3   863.19   829.33   407.20   93.420
      ZeroEnergy[kcal/mol]              8.0991247398917476
      ElectronicLevels[1/cm]            1
        0.0000000000000000              2.0000000000000000
    End
 !*****************************************
    RRHO          !           Structure 2
      Geometry[angstrom]          9
        C   -0.04019  -0.07057  -0.70690
        C   -0.04476  -0.07857   0.79923
        H    0.97075  -0.07764   1.19340
        H   -0.55966   0.79671   1.19340
        H   -0.55017  -0.96321   1.19127
        H    0.54959  -0.85383  -1.17585
        H   -1.01468   0.03758  -1.17586
        H    0.55696   0.97743  -1.05550
        H    1.05868   1.85871  -1.27020
      Core       RigidRotor
```

```
      SymmetryFactor    1.0000000000000000
    End
    Rotor                     Hindered
      Group                   6   7   8   9
      Axis                    1   2
      Symmetry                3
      Potential[kcal/mol]         4
        0.00    0.89    1.83    0.89
    End
    Frequencies[1/cm]         19
      3184.1   3135.7   3120.0   3105.2   3058.3   1499.9   1499.6   1470.9   1411.4   1353.3
      1321.9   1276.6   1219.2   1172.7   1039.7   864.60   829.58   440.07   166.31
    ZeroEnergy[kcal/mol]            8.5418081932175607
    ElectronicLevels[1/cm]          1
      0.0000000000000000            2.0000000000000000
  End
!*****************************************
  Tunneling   Eckart
    ImaginaryFrequency[1/cm]      1457.0200000000000
    WellDepth[kcal/mol]           $wdepfor
    WellDepth[kcal/mol]           $wdepback
  End
 End
!**********************************
End
!-------------------------------------------------------------------------------------------------------
```